CRYSTALLIZATION AND DISSOLUTION STUDIES OF CALCIUM OXALATE MONOHYDRATE: A MICROFLUIDIC APPROACH

By

MAGATA NKUBA

A thesis submitted to the

Graduate School-Camden

Rutgers, The State University of New Jersey

In partial fulfillment of the requirements

For the degree of Master of Science

Graduate Program in Chemistry

Written under the direction of

Dr. George Kumi

and approved by

_____

Dr. George Kumi

_____

Dr. Georgia Arbuckle-Keil

_____

Dr. Jinglin Fu

Camden, New Jersey

May 2018

THESIS ABSTRACT

Crystallization and dissolution studies of calcium oxalate monohydrate: a microfluidic approach

by MAGATA NKUBA

Thesis Director:

Dr. George Kumi

Calcium oxalate monohydrate (COM), the most stable hydrate of calcium oxalate (CaOx) at typical room temperatures and pressures, can produce undesirable effects in certain systems, such as kidney stone disease in humans, scale deposits in mechanical equipment, and patinas on art monuments. COM dissolution has been considered as a way to remove COM crystals in such systems. However, there are only a few, if any, effective solutions that can be used in the aforementioned systems. In this study, a microfluidic approach has been used to characterize the COM dissolution abilities of various dissolution agents in the pH range of 3-9. The dissolution agents consisted of eight carboxylic acid compounds: acetic acid, formic acid, DL-malic acid, succinic acid, citric acid, hydroxycitric acid, 1, 2, 3, 4-cyclobutanetetracarboxylic acid (H_4CBUT), and ethylenediaminetetraacetic acid (EDTA). COM crystals were synthesized and dissolved using two different microfluidic devices, namely a 3-input, 3-output device and a 1-input, 1-output device. Results demonstrate that EDTA, H_4CBUT, citrate, and hydroxycitrate have a relatively strong ability to dissolve COM crystals in the pH range of 7 to 9. At solution pH values of 5 and 7, acetate, succinate, EDTA, H_4CBUT, and citrate were

significantly more effective at COM crystal dissolution than the other solution examined. Succinate, malate, and acetate seemed to have no significant benefit. Overall, the number of carboxylic acid functional groups appeared to give an indication of which dissolution agent would be most effective at dissolving COM crystals. As expected, water alone exhibited relatively poor COM dissolution capabilities at pH values greater than 5.

Dedication

This thesis is dedicated to

My parents, the reason for who I have come to be today. My beloved spouse, Bijoux Bowena Kapambu, and children, Emilia Ndongo da Silva Nkuba, Hendrick Mukelenge da Silva Nkuba, Leonardo da Silva Nkuba, Joana da Silva Nkuba, and Dadiva Nia da Silva Nkuba, for your deep affection, great comfort, and sacrifice. Those people who always strive to survive in a world without pity, compassion, and sympathy.

Acknowledgements

I express my sincere gratitude to my advisor, Dr. George Kumi, my committee members, Dr. Georgia Arbuckle-Keil and Dr. Jinglin Fu, and all the faculty members of the chemistry department at Rutgers University who have contributed their time and suggestions from moment to moment in successfully completing this project.

Finally, Sonangol and Total Angola find here the expression of my honest gratefulness for their financial support, without which I could not achieve my goal.

Table of Contents

List of Figures

List of Tables

Chapter 1 Introduction

1.1 Calcium oxalate monohydrate (COM)

Calcium oxalate monohydrate (COM), the most stable hydrate of calcium oxalate (CaOx) at typical room temperatures and pressures, is a sparingly soluble salt in aqueous solutions. Its chemical formula is CaC_2O_4. Because of its low solubility, COM, like the other two known hydrates of CaOx, crystalizes spontaneously in various geochemical, biological and industrial environments. [1-2] In some of these systems, its formation produces undesirable effects, such as kidney stone disease in humans, [3-4] scale deposits in mechanical equipment, [5] and patinas on art monuments. [6-7] These effects can be costly to remediate. For example, the cost of treating kidney stone disease can be high, depending upon the procedure deemed necessary to remove the stone. [8] COM formation in industrial equipment leads to scale formation in pipes that is difficult to remove and is problematic because it has deleterious effects which include reduced heat transfer in heat systems, loss of production capacity, unscheduled shutdowns for scale removal and increased pumping costs. [5]

With respect to human healthcare, the pathological nature of COM has been known for over 200 years. [9] As a result, there are numerous studies on controlling its formation and understanding its properties. These efforts have resulted in many proposed solutions including increasing intake of water, [10] change in diet, [11-12] and drug therapy. [13] In industry, the deleterious effects of scale deposition have motivated the search for more viable scale removal strategies. [14-16]

Recently, several of these studies have focused on gaining a more microscopic understanding of the biomineralization process. In the healthcare field, these studies

include chelation therapy, [17-21] chemolysis therapy, [22] and renacidin treatments, [23] while for industrial applications such studies have focused on the dosage of specific antiscalants or the use of polymeric scale inhibitors. [16] The topic of calcium oxalate crystal dissolution continues to be a subject of investigation. [4, 12, 24-26]

1.2 COM dissolution

The majority of COM studies in the literature have focused on crystal growth. However, there have been a number of investigations on the dissolution of CaOx and of COM in particular. In fact, dissolution therapy has been considered as a way to remove kidney stones in mammals, and an effective COM dissolution method for scale in industrial equipment is also desired. For example, among the different treatments proposed by scientists, dissolution therapy has emerged as one of the most effective methods to treat uric acid stones. [21, 27] This therapy has also been tested in the study of calcium phosphate stones, [22] struvite, [28] and cystinuria diseases. [29] Other findings show that calcium ions, which are the metal ions in COM crystal structures, display a good affinity for oxygen ligands compared to other metals such as beryllium, magnesium, and zinc. It has also been reported that Ca ions general adopt coordination numbers between six to eight in crystal structures. [30] Chelating therapy has been increasingly utilized in various treatments, including iron chelating therapy to cure thalassemia [20] and metal chelating treatment for Alzheimer's [17-18] and atherosclerosis. [31-32]

As recent studies show, there is still progress to be made in order to attain a level of understanding that can prevent COM formation, particularly in complex environments like the human urinary tract. [33-34] Kidney stone disease is on the rise, [35] and the sooner these advances are attained the better the options for treating this disease will become. [33]

While dissolution therapy is a treatment routinely used to prevent or dissolve uric-based urinary stones, [21-22] no such treatments exist for CaOx. In other words, the limited dissolution agents currently known (including Ethylenediaminetetraacetic acid (EDTA), citric acid, polyacrylic acid) are not viable candidates for such medical applications. [36-37]

Conjugate bases of neutral carboxylic acids (i.e., the fully or partially deprotonated forms of these acids) contain one or more carboxylate ions, and these carboxylate-ion-bearing species are known to be effective calcium chelators. In other words, they have the capability to dissolve COM crystals. [21, 38-39] Carboxylic acids are generally known as weak acids. In aqueous solutions, they can form carboxylate ions as a result of proton transfers. Among the carboxylic acids investigated, EDTA is known to bind Ca^{2+} in a manner that forms a complex, thereby reducing the "free Ca^{2+}" in solution. EDTA is an amino carboxylic acid (Figure 1), and it binds tightly to metal cations (e.g., Ca^{2+}, Fe^{2+}, Cu^{2+}) using four carboxylate ions and two amine groups. [33, 36, 40-42]

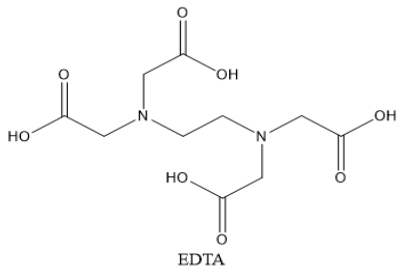

Figure 1. Structure of EDTA: hexadentate ligand (4 carboxylic groups and 2 nitrogen atoms).

There are other carboxylic acid agents capable of dissolving COM crystals, including biomolecules containing aspartic or glutamic acids, [40, 43] osteopontin, [44] protein transferrin, [45] and polycarboxylic organic acids. [33, 43, 46-50] A few comparisons of the dissolving abilities of these agents have been reported. [21, 36, 47] Chutipongtanate et al. report that citrate had a greater impact on COM dissolution (by reducing crystal size,

number, and total crystal mass by 37%, 53% and 72% respectively when contrasted to blank and negative controls) than phosphate. [33]

1.3 COM structure and properties

CaOx crystals are mostly observed in plant tissues, microorganisms, urinary stones, and sediments. Depending on the hydration state, calcium oxalate crystals exist naturally in three polymorphic forms: $CaC_2O_4 \cdot H_2O$, called calcium oxalate monohydrate (whewellite); $CaC_2O_4 \cdot (2+x)H_2O$ with $x < 0.5$, called calcium oxalate dihydrate (weddellite); and $CaC_2O_4 \cdot (xH_2O)$ with $3 > x > 2.5$, known as calcium oxalate trihydrate (caoxite). [51]

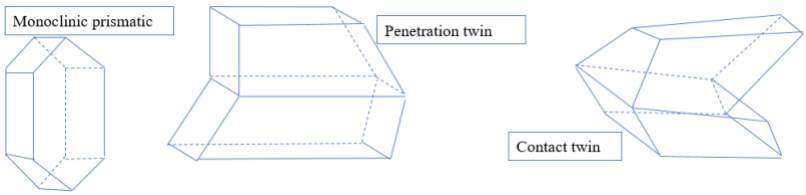

Figure 2. Examples of COM crystal habits

COM is the most predominant CaOx form. Thermodynamically, it is the most stable, with a solubility product of 1.66×10^{-9} at 25ºC at an ionic strength of 0.15 M. [52] It can have a prismatic habit as a single crystal. However, the most common form involves twinning, which frequently occurs on the $(\bar{1}00)$ face. [53] COM is found as penetration twins (interpenetration of single crystals) or contact twins (the planes have a defined composition), as shown in Figure 2.

Three crystalline structures for COM have been reported. However, COM is typically found as monoclinic $P2_1/c$ crystal. One reported polymorph is an elementary structure stable over 45ºC that is a monoclinic crystal; it belongs to space group $P2_1/n$ with n defining a diagonal glide. P refers to one lattice point per unit or primitive unit cell, the

number *2* implies a two-fold screw axis along the *b* axis, and 2_1 represents a rotation of 180º followed by a translation along the screw axis. Each unit cell possesses eight formula units. Its lattice parameters are *a* = 9.978 Å, *b* = 7.295 Å, *c* = 6.292 Å, and β =107.07º. [53-54] Below 45ºC is a derivative structure with *a* = 9.9763 Å, *b* =14.5884 Å and *c* = 6.29134 Å, *β* = 107.05º. The arrangement of oxalate ions in the plane (010) increases the unit cell dimensions and causes the symmetry to become into space group $P2_1/c$. Here, *P* refers to one lattice point per unit or primitive unit cell, the number *2* means a two-fold screw axis along *b*, 2_1 means a rotation of 180º followed by a translation along the screw axis and *c* refers to the operation of a glide plane along axis *c* which includes a reflection in the plane (*a, c*) accompanied by a translation along the *c* axis. [53] Between 118ºC and 130ºC the third crystalline structure appears, called the new COM phase. This new COM phase pertains to the orthorhombic system and belongs to space group *mmm*. Its lattice parameters are: *a* = 12.088 Å, *b* = 10.112 Å , *c* = 14.634 Å (see appendix). [52]

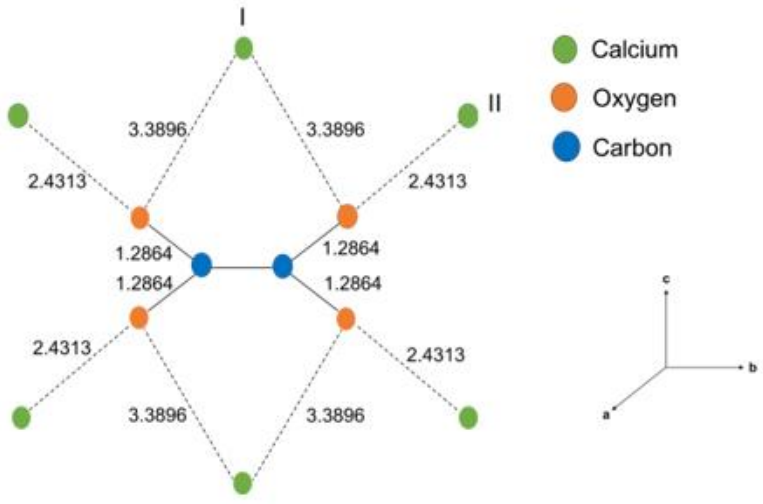

Figure 3. Calcium oxalate bonds in COM crystal: chelate bond (calcium-oxygen bonds) and covalent bond (carbon-carbon and carbon-oxygen bonds). Bond lengths are given in Angstrom (Å). [55]

Growth conditions (for example, ionic strength, pH, temperature, and local environment) affect the structure and size of COM crystals. [56] The characterization of the geometry of COM crystals indicates that the oxalate molecules are planar, as indicated in Figure 3. The carbon-carbon bond of the oxalate ions is not directly linked to the Ca^{2+} ions. The latter occupy two different sites within the COM crystal. The bond between the Ca^{2+} (I) and each of the two oxygens of the oxalate ion is a chelate bond (bond length: 2.3896 Å). The Ca^{2+} (II) interacts only with one oxygen of a specific oxalate ion. This Ca^{2+} (II) interaction leads to a bond measuring approximately 2.4313 Å (Figure 3). The third and generally weak type of interaction existing in COM crystals is hydrogen bonding. These bonds form between one or two hydration waters and the oxygen of an oxalate ion (Ox^{2-}).

1.4 Research objective

The dissolution process of COM crystals is poorly understood. There is also a lack of viable COM dissolution mixtures for medical and industrial applications. There does not appear to be any work characterizing the relationship between the dissolution capabilities of a mixture and the specific type (mono, di, tri, tetraprotic acids) or form (fully or partially ionized) of the carboxylic acid dissolution agent present in the mixture. In fact, even the few studies comparing the dissolution capabilities of some carboxylate acids either do not account for the effects of solution pH [21, 23, 57] or only undertake this comparison in a narrow solution pH range. [34, 36-37, 47-48] Most of these studies use mixtures that are complex (have more than one possible dissolution agent). [48, 58] While direct comparisons about such solutions can be made, it is impossible to (1) identify the primary agent responsible for the enhanced COM dissolution abilities or (2) extract mechanistic

details about the dissolution process. The number of carboxylate ion (COO^-) groups present in a system depends upon the specific acid and on the solution pH. Because the oxalate ion (Ox^{2-}) is a deprotonated form of oxalic acid, the form of Ox^{2-} in solution also depends on pH. Thus, pH does play a role in the COM dissolution process.

Currently, it is also not clear whether a known carboxylic acid growth inhibitor for COM can also favor the dissolution of COM. [59] Indeed, whether a specific growth inhibitor will exhibit dissolution capabilities in any chemical environment depends upon the mechanistic details of crystal growth inhibition versus crystal dissolution. [60] Calcite dissolution studies show that there can be distinct kinetic and mechanistic differences between growth and dissolution. [61] In fact, there are indications that a COM growth inhibitor may suppress the dissolution of some specific crystal planes. [62]

The work presented here focuses on furthering the current understanding of COM dissolution by characterizing the relationship between the dissolution abilities of various carboxylic acids and the acid type. Specifically, to establish the correlation, if any, between dissolution ability and acid type (mono, di, tri, or tetra protic), this study determines the COM dissolution abilities of eight carboxylic acid types in a pH range of 3-9. Some of the key questions of this study include:

(a) Is there a correlation between pH values of a solution of specific carboxylic acid and its capability to dissolve COM crystals?

(b) If this correlation exists, by using a specific carboxylic acid or combination of carboxylic groups, at which pH value of the solution is its capacity for dissolving COM crystals more effective?

(c) Does the capability of dissolving COM crystals depend on the number of carboxylic groups present in the dissolution agent or does the efficiency of the dissolution agents rely on the ionized carboxylic acid form (fully or partially ionized)?

(d) How can the capability of the dissolution agent be tuned by modifying the pH values of a medium if we keep the concentration of the solution constant?

1.5 Thesis outline

The current state of understanding and advances with respect to COM dissolution were presented in Chapter 1, as were the questions and objectives guiding this study. Chapter 2 details the experimental methods and protocols applied to explore the dissolution of COM crystals. Chapter 3 describes and discusses the experimental results achieved in this investigation, and Chapter 4 offers a summary of the research and directions for future investigation.

Chapter 2 Experimental Methods and Procedures

2.1 Materials

All the materials used in this study were purchased from Sigma Aldrich, Alfa Aesar, and Fischer Scientific. All reagents were used as purchased. Table 1 below reports the product name, formula, purchasing source and purity. All aqueous solutions utilized in this research were prepared with deionized water filtered twice or with 18 mΩ water.

Name of product	Formula	Source	Purity
Calcium oxalate monohydrate	$CaC_2O_4.H_2O$	Alfa Aesar	99 %
Potassium oxalate monohydrate	$K_2C_2O_4.H_2O$	Sigma-Aldrich	99.5-101.0 %
Calcium chloride	$CaCl_2$	Sigma-Aldrich	≥ 93.0 %
1,2,3,4-Cyclobutanetetracarboxylic acid	$H_4C_4(CO_2H)_4$	TCI-America	> 98.0 %
Potassium hydroxycitrate tribasic monohydrate	$H_5K_3C_6O_8.H_2O$	Sigma	95.0-105.0 %
DL-Malic acid disodium salt	$H_4Na_2C_4O_5$	Aldrich	≥ 95 %
Sodium formate	$HNaCO_2$	Aldrich	99.998 %
Sodium acetate trihydrate	$NaCH_3CO_2.3H_2O$	Fischer Scientific	99.0-101.0 %
Sodium citrate dihydrate	$H_5Na_3C_6O_7.2H_2O$	Fischer Scientific	99.0-101.0 %
Succinic acid disodium salt	$H_4Na_2C_4O_4$	Aldrich	99.0 %
Sodium hydroxide	NaOH	Fischer Scientific	98 %
Hydrochloric acid	HCl	Sigma-Aldrich	37 % HCl in H_2O
Ethanol	H_6C_2O	Sigma-Aldrich	99.5 %
Ethylenediaminetetraacetic acid (EDTA)	$H_{14}Na_2C_{10}O_8N_2.2H_2O$	Fischer Scientific	99.0-101.0 %

Table 1. List of chemicals used for this study

2.2 Microscopy

Two different optical microscopes were used in this study to perform the COM crystallization and dissolution processes. First, a Bausch & Lomb optical microscope (Stereo Zoom 4) was utilized to observe the formation of COM crystals within the microfluidic crystallization device, that is, to monitor the evolution of the crystallization process inside the microfluidic device. This stereomicroscope was equipped with a camera (Moticam 5.0 MP) to facilitate the observation of COM crystals and the collection of optical images. Second, an Olympus (BX41) Optical equipped with a 50X objective was used to monitor the process of dissolution via a camera attached to Horiba Raman Microscope. However, Raman microscopy was not used for this study.

2.3 Microfluidic device fabrication

2.3.1 Crystallization device fabrication

Devices were made using a previously described protocol [63] that will be briefly described here. UV photolithography and soft lithography techniques were used to create microfluidic devices needed for this study: one for crystallization and another for dissolution of COM crystals. To form the crystallization microfluidic device with soft lithography, an acrylate master microstructure was necessary. Layers of scotch tape were used as spacers on a fluorocarbon-functionalized slide (to achieve the desired film height). Then, approximately 3 to 5 drops of a photoresist were placed on the surface of the slide. An acrylate-functionalized slide was placed on the top of the fluorocarbon-functionalized slide, and a transparency mask was used to create the desired exposure to UV light (Black-Ray B-100A, UVP) for about 3 minutes (Figure 4). Following this exposure, the two slides were separated and acetone was used to remove the residual

resin that was not exposed. Two successive acetone baths (1 minute each) were used for this removal. [63]

To finalize the creation of the device, the slide containing the master structure was put on a piece of aluminum foil and the latter was folded into the form of an open box. The PDMS pre-polymer mixture was poured onto the master structure. The assembly (i,e., the PDMS pre-polymer mixture, the master structure, and the foil) was heated for 5 hours at 75ºC to cross-link the polydimethylsiloxane (PDMS). Next, the PDMS mold was separated from the slide, the mold's edges were cropped, and six holes were bored (Harris Unicore, 1.20 mm) to fit the 6 plastic tubes (3-input, 3-output tubes).

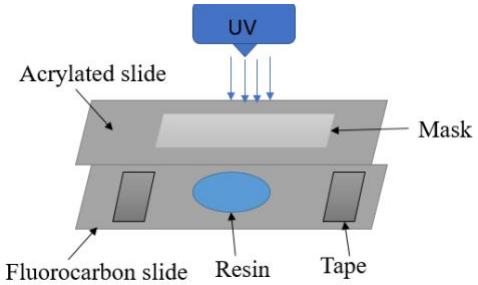

Figure 4. The UV photolithography process to obtain a master structure; all slides were exposed to UV radiation through a mask. [63]

Then, one flat piece of cured PDMS and the PDMS mold were put together. The flat piece of cured PDMS was obtained by following the same procedure used to fabricate the PDMS mold, except no master structure was on the slide put in the aluminum foil. Instead, a fluorocarbon-functionalized slide was placed into the aluminum foil. Oxygen plasma-cleaning PDC-32G (Harrick Plasma) was conducted (~30 sec, ~600 mTorr O_2) to immediately bind the two PDMS pieces (the mold and flat portion). After these pieces

were pressed together, plastic tubes were then connected into the open holes of the device.

2.3.2 Dissolution device fabrication

To make the dissolution device, several layers of glass were cut from a microscope slide (6 glass squares of 1.5 x 0.5 cm each). [63] Three layers of small glass squares were placed at each extremity of a silicon slide (Figure 5 a and b). Then, the entire assembly was put into an aluminum foil box, which was then filled with PDMS pre-polymer solution. This assembly was later heated for approximately 30 minutes. Subsequently, the PDMS mold was pulled apart from the microscope slide. Next, two holes were bored into the mold to fit two tubes (Harris Unicore, 1.20 mm); one served as the way in and the other as the way out through the microfluidic dissolution device. For each experiment, a glass coverslip was used to cover the upper side of the microfluidic dissolution device. It was attached with scotch tape to the PDMS to avoid solution leakage.

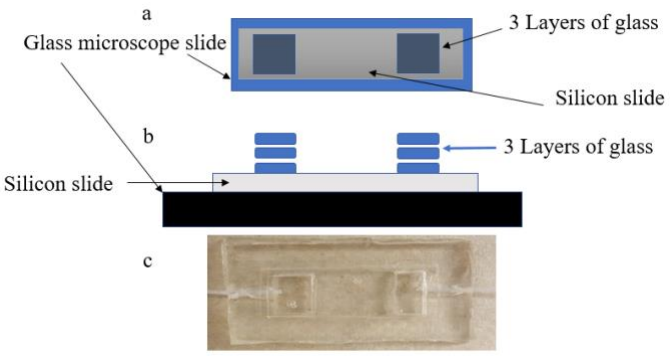

Figure 5. a) A schematic of microfluidic dissolution device fabrication. b) Master structure of microfluidic dissolution device. c) An optical image of the microfluidic dissolution device. [63]

2.4 COM crystallization

The COM crystals used to explore the COM dissolution process were created using a microfluidic crystallization device. As per a developed protocol, [64] the microfluidic crystallization device (Figure 6 a) was placed into an ethanol bath, and this bath was then placed into a desiccator, which was evacuated for 30 minutes to remove or reduce the amount of air inside the porous PDMS device. After 30 minutes, the device was placed onto the stereomicroscope to facilitate monitoring of the crystallization process.

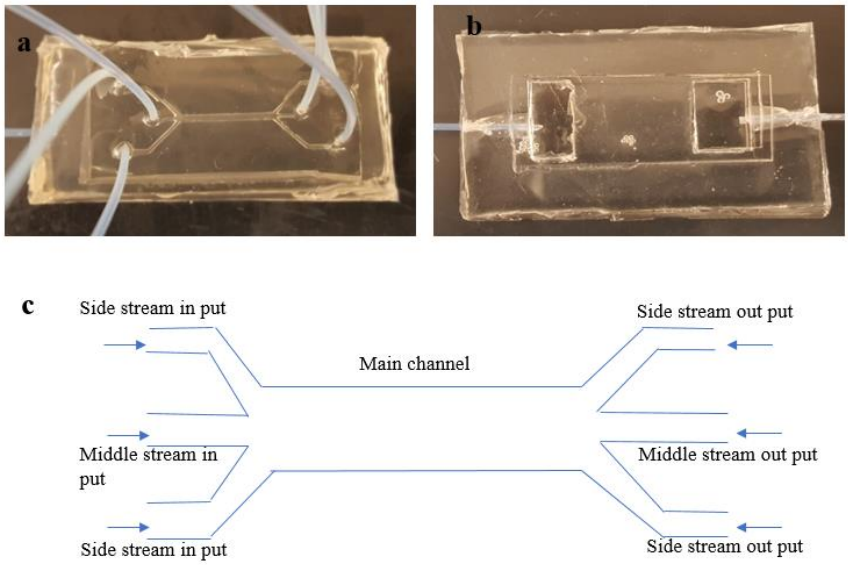

Figure 6. a) Microfluidic device 3-input, 3-output for COM crystallization, b) Microfluidic device 1-input, 1-output for COM crystals dissolution, c) Schematic of microfluidic device for crystallization (3-input, 3-output microfluidic device).

The input side of the device, consisting of 3 inputs, was used to load solutions into the device, while the output side was used to remove waste and collect the crystals (Figure 6 c). All output tubes were placed into separate solutions, namely deionized water (contained in beakers). The middle stream output beaker contained a supersaturated

solution of COM to prevent the COM crystals from dissolving in the collection solution after they formed in the device. The two side stream outputs were collected in separate beakers simply for convenience. To further prepare the device to produce COM crystals, ethanol was passed (~10 min, 100 µL/min) through the device to remove any air bubbles inside the tubes and the microfluidic device. Water was than used to flush out the ethanol. Dyes were injected after the water to visualize the flow profile of the liquids inside the microfluidic device (Figure 8 a). Then, another water flush was used to remove the dye solutions from the device. Removal of the dye was followed by the pumping of 120 mM of potassium oxalate monohydrate ($K_2C_2O_4.H_2O$) and 120 mM of calcium chloride ($CaCl_2$) into the microfluidic device from the two different side stream inputs while simultaneously pumping water through the middle stream input (Figure 6 c and Figure 7). In this configuration, the middle stream is where the COM crystals form.

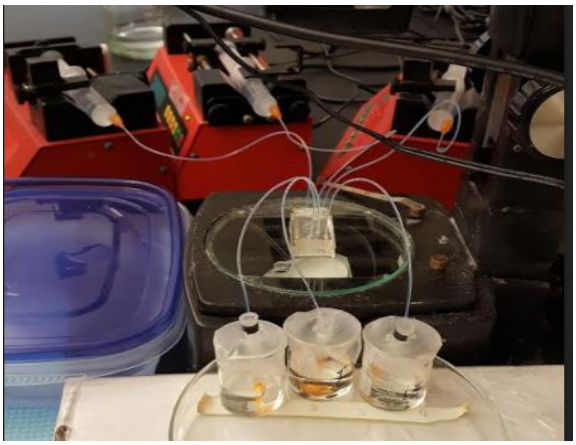

Figure 7. Photo image of COM crystallization set-up.

Upon introduction of the salt solutions, a line of crystals appeared in the middle of the device (Figure 8 b). The appearance of this line depended upon the time taken for the salt solutions to travel from their respective syringes to the device channel (via the input

tubes). After 20 minutes of crystallization (i.e., 20 minutes after the crystal line was detected), the middle stream output collection beaker containing a glass slide was substituted with a new beaker containing a new collection slide immersed in a supersaturated COM solution to avoid the dissolution of COM crystals leaving the device. The collection of the sample took another 20 minutes before the end of the process of crystallization. All collection slides containing COM crystals were removed

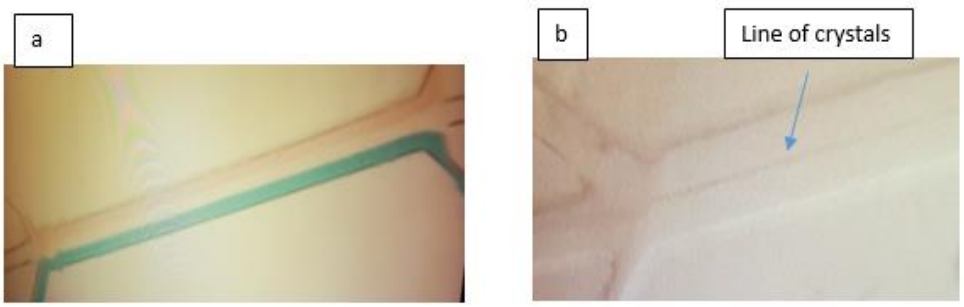

Figure 8. Optical image of liquid profile (a) and line of COM crystals (b).

from their beakers and dried at room temperature immediately after the beaker was separated from the output tubing. At the end of each crystallization experiment, 1 M HCl was injected through the device to dissolve any residual COM crystals and prepare the microfluidic device for the next experiment. Water was then flushed through the device. To be consistent with the size of the COM crystals produced, the same device was utilized. The size of CaOx crystals varied from one slide to another depending on the quantity deposited on a specific area of slide after 20 minutes.

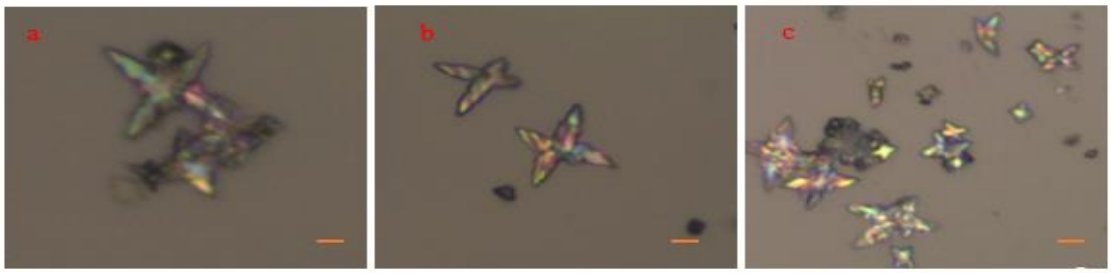

Figure 9. Optical images of different COM crystal shapes: (a) x-shaped, (b) x-shaped and agglomerate crystals, and (c) dendrite. The scale bars shown are 4 µm. Crystals shown range from 4 to 20 µm.

2.5 COM dissolution

COM crystal dissolution studies were undertaken in a microfluidic dissolution device (Figure 6 b). This PDMS device was a 1-input-1-output device (Figure 5 c and Figure 6 b). Sections (~2.5 mm^2) of the dried collection slides (i.e., containing COM crystals) were placed into the dissolution device and irrigated with specific solutions during these studies. As COM crystals had different sizes, the stereomicroscope equipped with a camera (Moticam 5.0 MP) was used to facilitate the identification and selection of COM crystals (X-shaped) used for experiments. Only COM crystals with approximately similar sizes (around 4 to 20 µm) were selected for this study. Double-sided tape was used to mount this glass inside the dissolution device. For each experimental trial of a particular carboxylic acid, a 5 mM solution with a known pH was passed (200 µL/min) through the device via syringes and syringe pumps (New Era, NE-1000 or Kent Scientific Genie Plus). Both were set at the same rate (i.e., 200 µL/min). HCl (~0.1M) and NaOH (~0.01M) stock solutions were prepared and used to fix the pH of any carboxylate acid solution at a specific pH. The volumes of HCl and NaOH used were small (~0.1 ml) compared to the amount of acid solutions prepared (~100 ml) and did not change the formal concentration of the carboxylic acid solutions. The entire process of dissolution

(Figure 10) for each particular carboxylic acid solution was visualized using a camera that recorded images every two minutes. Each experimental trial was conducted at least three times. The end of experiment occurred when the COM crystal or group of COM crystals were totally dissolved as determined from the optical image of the camera. Any crystal that "washed away" during the dissolution process was not used for the study. The images were collected using a 50X objective (section 2.2).

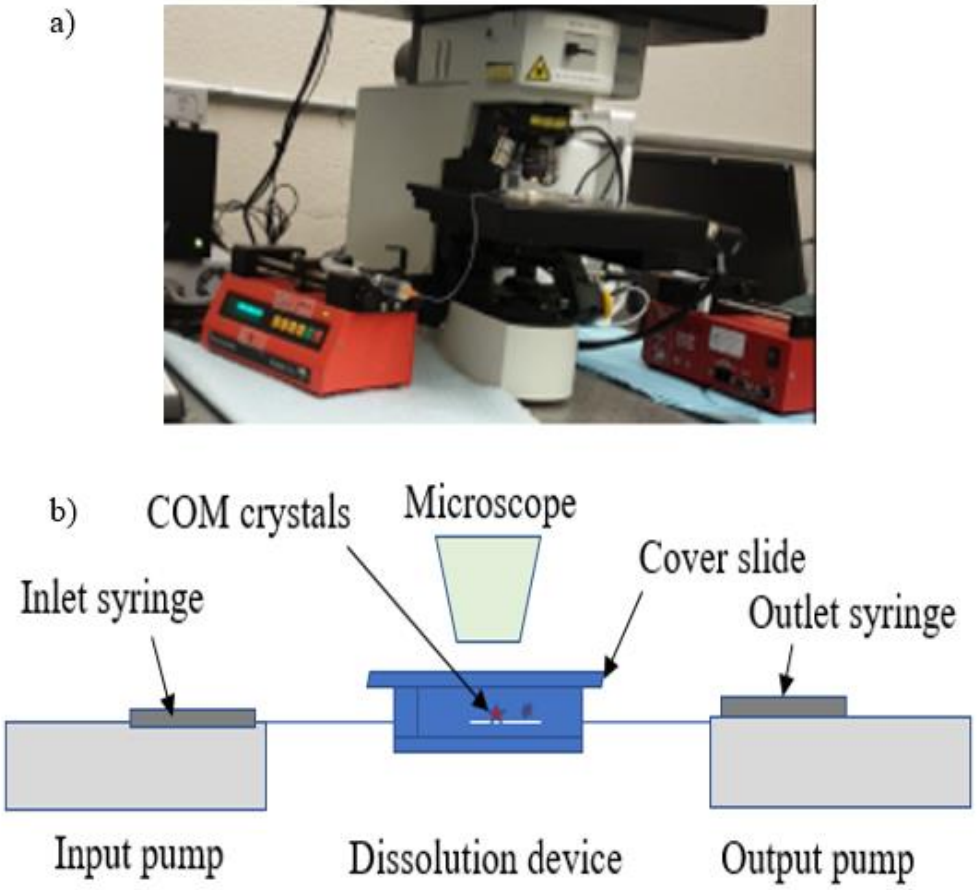

Figure 10. Dissolution process. a) Optical image of dissolution experimental setup. b) Schematic of COM crystal dissolution process.

Chapter 3 Results and discussions

3.1 Introduction

In this study, a microfluidic device approach was used to characterize the COM dissolving capabilities of various solutions containing carboxylic acids as dissolution agents or solution additives. For any carboxylic acid, the specific chemical form or species of the acid that exists in an aqueous solution depends upon the solution pH. Therefore, the COM dissolution ability, of the eight dissolution agents used in this work (Figure 11), was quantified at various solution pH values.

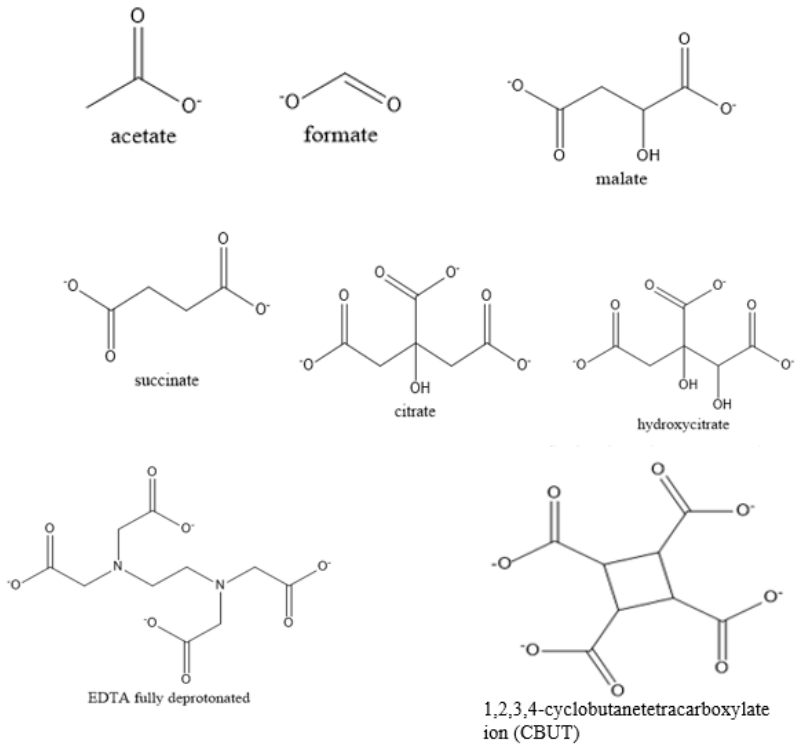

Figure 11. Structural illustration of the fully deprotonated anionic dissolution agents used in this study.

The speciation reactions and dissolution constants for these agents are listed in Table 2. COM crystals were synthesized in a crystallization microfluidic device, while the dissolution experiments were conducted in a dissolution microfluidic device. Optical

images of the dissolution process were captured at two-minute intervals using a camera attached to a stereomicroscope. Except for 1,2,3,4-cyclobutanetetracarboxylic acid (H_4CBUT), all the dissolution agents used in this research are sodium salts.

Equation	Compound	pKa
$C_2H_4O_2 \rightleftharpoons C_2H_3O_2^- + H^+$	acetate	4.75
$CH_2O_2 \rightleftharpoons CHO_2^- + H^+$	formate	3.75
$C_4H_6O_5 \rightleftharpoons C_4H_5O_5^- + H^+$	malate	3.40
$C_4H_5O_5^- \rightleftharpoons C_4H_4O_5^{2-} + H^+$	malate	5.11
$C_4H_6O_4 \rightleftharpoons C_4H_5O_4^- + H^+$	succinate	4.21
$C_4H_5O_4^- \rightleftharpoons C_4H_4O_4^{2-} + H^+$	succinate	5.64
$C_6H_8O_7 \rightleftharpoons C_6H_7O_7^- + H^+$	citrate	3.13
$C_6H_7O_7^- \rightleftharpoons C_6H_6O_7^{2-} + H^+$	citrate	4.76
$C_6H_6O_7^{2-} \rightleftharpoons C_6H_5O_7^{3-} + H^+$	citrate	6.40
$C_6H_8O_8 \rightleftharpoons C_6H_7O_8^- + H^+$	hydroxycitrate	2.90
$C_6H_7O_8^- \rightleftharpoons C_6H_6O_8^{2-} + H^+$	hydroxycitrate	4.29
$C_6H_6O_8^{2-} \rightleftharpoons C_6H_5O_8^{3-} + H^+$	hydroxycitrate	5.11
$H_4Y \rightleftharpoons H_3Y^- + H^+$	EDTA (H_4Y)	2.00
$H_3Y \rightleftharpoons H_2Y^{2-} + H^+$	EDTA (H_4Y)	2.70
$H_2Y^{2-} \rightleftharpoons H_1Y^{3-} + H^+$	EDTA (H_4Y)	6.20
$H_1Y^{3-} \rightleftharpoons Y^{4-} + H^+$	EDTA (H_4Y)	10.30
$H_4CBUT \rightleftharpoons H_3CBUT^- + H^+$	H_4CBUT	Not known
$H_3CBUT^- \rightleftharpoons H_2CBUT^{2-} + H^+$	H_4CBUT	Not known
$H_2CBUT^{2-} \rightleftharpoons H_1CBUT^{3-} + H^+$	H_4CBUT	Not known
$H_1CBUT^{3-} \rightleftharpoons CBUT^{4-} + H^+$	H_4CBUT	Not known

Table 2. Speciation Reactions and dissociation constants for the polyprotic acids. [48, 65-68] Not known signifies data that is not accessible in the published writings. H_4Y represents EDTA and Y^{4-}, the completely deprotonated anion of EDTA.

For all dissolution experiments, the flow rate of the dissolution solution was 200 µL/min, and the dissolution agent concentration for each solution was 5 mM; this concentration was selected based on previous study [33] that demonstrated that certain carboxylic acid solutions with this concentration dissolved small (~10 µm) COM crystals within a period of approximately 60 min. The dissolution times reported in this work are an average of three replicate dissolution experiments. Also, the experimental conditions were similar for all experiments. For example, each trial was performed at room temperature with room-temperature solutions.

3.2 COM dissolution in water

3.2.1 Dissolution mechanism of solids

The dissolution behavior of solids is generally characterized by three different terms: (1) transport-controlled, (2) interface-controlled, and (3) mixed-kinetic-controlled. These terms refer to three distinct mechanisms, and each of these mechanisms is based on two processes: an interfacial step and a mass transport step. The interfacial step is defined by the solvation of solid state of molecules, while the transport step determines the transport of dissolved molecules into the bulk of solution. [37, 69] A minimum of three scenarios exists. If the rate of the interfacial step is smaller than the rate of the transport step, the solution concentration near the surface of solid is less than its maximum solubility in that solution. The rate of the overall process is limited by this interfacial step, and the dissolution mechanism is said to be interface-controlled. Conversely, if the interfacial process occurs much faster than the transport of dissolved molecules into the bulk of solution, then mass transport is the rate-determining step of the process. [34, 48] Transport-controlled is the term used to describe such processes. If both, interfacial and

transport steps have similar rates, then neither interfacial step nor transport step is the rate-limiting step of the process; the term mixed-kinetic-controlled is used to describe such processes. [70]

3.2.1.1 Transport-controlled dissolution

Noyes et al. investigated the phenomena of transport-controlled dissolution mechanism (Figure 12). [71] They concluded that the dissolution rate is a function of the difference between the solubility of a solid and its bulk concentration in solution. They represented the relation between the dissolution rate and this difference by the expression,

$$dM / dt = k(C_s - C_b) \quad (3\text{-}1)$$

where, dM / dt defines the rate of quantity of particles dissolving per unit time. C_s, C_b, k represents the solubility, the bulk concentration, and the dissolution rate constant, respectively. This theory was unsuccessful, as it could not explain the relation between the rate constant and transport properties of the solute. [71] To give a physical significance to the above expression, Nernst [72] and Brunner [73] suggested a correction. They suggested that the solute diffuses from the solid surface to the bulk solution through a stagnant layer forming a linear concentration profile. [70, 74-75] This correction simplified the meaning of rate constant by combining the hydrodynamic complexities into the diffusion layer. The rate constant k becomes

$$k = AD / h \quad (3\text{-}2)$$

where A, D, and h define the solid surface area, diffusion coefficient, and diffusion layer thickness, respectively. Unfortunately, the introduction of a stagnant layer did not permit

theoretical calculation to proceed without knowing the value of the thickness of the diffusion layer. This value must be obtained from dissolution rate data.

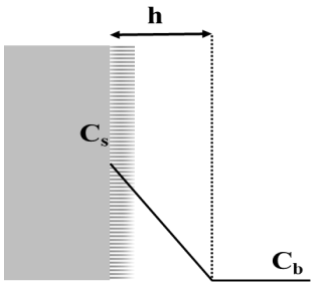

Figure 12. Nernst diffusion layer model for dissolution from a planar surface, Cs = solubility, Cb = bulk solution concentration, and h= diffusion layer thickness. [76]

3.2.1.2 Mixed-kinetic-controlled dissolution

When both interfacial step and transport step rates are similar, the rate of dissolution is calculated from the mass transport properties and physicochemical parameters associated with the kinetic processes of solubility and deposition. Rickard et al. reported a general accepted model for mixed-kinetic-controlled dissolution. They proposed equations for both steps separately. The interfacial reaction rate is given by

$$J_c = k_c\,(C_s - C_o)^n \tag{3-3}$$

where, C_o, k_c are the concentration adjacent to the solid surface and "chemical rate constant," respectively. And the transport reaction rate is expressed by,

$$J_T = k_T\,(C_o - C_b) \tag{3-4}$$

where, k_T defines the transport rate constant.

At steady-state, Jc is equal to J_T and considering n=1, the dissolution rate [77] is represented by

$$J = Jc = J_T = [Jc\ J_T / (Jc + J_T)]\ (Cs - Cb) \quad (3\text{-}5)$$

3.2.2 CaOx chemical equilibrium and dissolution

Regardless of the specific mechanism, the solubility of a solid in a solution plays a role in the dissolution process. In transport-controlled and mixed-kinetic-controlled processes, this role is a particularly important one. COM dissolution has been reported to occur by a transport-controlled mechanism in certain initial calcium and oxalate ion concentration ranges. [78] Thus, understanding the solubility of CaOx in a specific solvent is constructive when examining dissolution kinetics.

3.2.2.1 CaOx precipitation

The equilibrium equation of CaOx described by the following Equation

$$CaOx(s) \rightleftharpoons Ca^{2+} + Ox^{2-} \quad (3\text{-}6)$$

characterizes the presence of Ca^{2+} and Ox^{2-} ions in solution. In agreement with general definition, the Ksp for CaOx is defined as the product of the Ca^{2+} activity, $a_{Ca^{2+}}$, and the Ox^{2-} activity, $a_{Ox^{2-}}$. Therefore, it is represented by

$$Ksp = a_{Ca^{2+}} \cdot a_{Ox^{2-}} = \gamma_{Ca^{2+}} [Ca^{2+}] \cdot \gamma_{Ox^{2-}} [Ox^{2-}] \quad (3\text{-}7)$$

where, $\gamma_{Ca^{2+}}$ and $\gamma_{Ox^{2-}}$ represent the activity coefficients of the calcium and oxalate ion, respectively. The square brackets define the amounts (i.e., dimensionless value) of the concentration (molar concentration values only) of Ca^{2+} and Ox^{2-} species in moles/L. If the activity coefficients associated with Equation (3-7) are neglected or are assumed to be equal to one, Equation (3-7) can be re-written as

$$Ksp = [Ca^{2+}] \cdot [Ox^{2-}] \quad (3\text{-}8)$$

This assumption is true only in solutions of low ionic strength.

In thermodynamics, the value of Gibbs free energy (ΔG) indicates if the chemical reaction is spontaneous, not spontaneous, or at equilibrium. With ΔG < 0, the chemical reaction is favored to proceed spontaneously at constant pressure and temperature. In general, ΔG does not indicate the kinetics of the process, i.e., how quickly the reaction will proceed. However, when ΔG = 0, it is an indication that the reaction has reached chemical equilibrium. Furthermore, the reaction cannot proceed without the energy. The relationship that exists between Gibbs free energy (ΔG), Gibbs standard energy (ΔG°) and the reaction quotient, Q, via the well-known expression

$$\Delta G = \Delta G^o + RTlnQ \tag{3-9}$$

where *R* and *T* are respectively defined as ideal gas constant in units of J/mol-K and temperature in Kelvin. *Q* is the reaction quotient at any moment in time. Considering a stoichiometrically balanced equation with four species A, B, C, and D:

$$wA + xB \rightleftharpoons yC + zD \tag{3-10}$$

The reaction quotient for this system at any moment in time is equal to

$$Q = \frac{a_C^y a_d^z}{a_A^w a_B^x} = \frac{\gamma_C^y [C]^y \gamma_D^z [D]^z}{\gamma_A^w [A]^w \gamma_B^x [B]^x} \tag{3-11}$$

where, w, x, y, and z are the values of stoichiometric coefficients in the chemical equation. As mentioned above, the driving force responsible for a chemical reaction is zero (ΔG = 0) when the process attains equilibrium. Consequently, the reaction quotient Q evaluated at equilibrium is exactly equal to the equilibrium constant, K. The reaction quotient is usually described by the following expression:

$$Q = \frac{[C]^y\,[D]^z}{[A]^w\,[B]^x} \tag{3-12}$$

As mentioned above, when ΔG = 0, Q = K, and this leads the Δ*G* relation

$$0 = \Delta G^\circ + RTlnQ \quad \Rightarrow \Delta G^\circ = -RTlnQ_{eq} = -RTlnK \tag{3-13}$$

When Equation (3-13) is substituted into Equation (3-9), one obtains

$$\Delta G = RTln(Q/K) \tag{3-14}$$

The Equation (3-13) enables the determination of the equilibrium constant from the standard-state free energy of reaction, or vice versa.

For CaOx, the free energy relationship becomes

$$\Delta G = RTln\frac{[Ca^{2+}][Ox^{2-}]}{Ksp} \tag{3-15}$$

In this equation, $[Ca^{2+}]$ and $[Ox^{2-}]$ are the values of the calcium and oxalate ion molar concentration at some specified time. The supersaturation ratio S is expressed as

$$S^2 = Q / Ksp \tag{3-16}$$

The magnitude of S depends on the Q/Ksp ratio. As a result, when S > 1, it implies that Q/Ksp > 1 and thus ΔG >0. In this situation, the process proceeds to produce more CaOx(s) rather than generating or dissolving more calcium and oxalate ions. The precipitation of these species to form CaOx solid is the thermodynamically favored reaction in this case. Solutions with S > 1 are supersaturated. Therefore, the determination of S allows the evaluation of whether or not favorable conditions for precipitation have been reached.

3.2.2.2 CaOx dissolution in water – theoretical considerations

While CaOx dissolution is of importance to processes aimed at removing COM crystals, there appear to be a relatively small number of studies associated with the effect of pH on the solubility of COM, even in pure water which is a relatively simple solvent system. The study made by McComas et al. related to CaOx solubility in pure water concluded that, "as the equilibrium between CaOx and its saturated solution is reached relatively quickly, any errors occurring in the CaOx solubility determinations are probably due to the CaOx". [79] They proposed the following Equation of solubility of calcium oxalate in any solution [80]

$$[Ca^{2+}]T = S' \frac{(H^+)+K_2'}{K_2'} \tag{3-17}$$

where $[Ca^{2+}]$ defines the concentration of Ca^{2+} and (H^+) is the activity of H^+. T represents the total concentration of oxalate (for example, the sum of $[Ox^{2-}]$ meaning concentration of $C_2O_4^{2-}$ and $[HOx^-]$ representing the concentration of $HC_2O_4^-$). S′ and K_2' defined as the solubility product of calcium oxalate and the second ionization constant of oxalic acid, respectively. K_2' is represented by the expression

$$K_2' = \frac{(H^+)[Ox^{2-}]}{[H0x-]} \tag{3-18}$$

When calcium or oxalate species are not in excess in the solution, the solubility is expressed by

$$L = [Ca^{2+}] = T \tag{3-19}$$

where L defines the solubility of calcium oxalate in moles per liter. The combination of (3-17), (3-18), and (3-19) yield

$$L = \sqrt{S' \frac{(H^+)+K_2'}{K_2'}} \quad (3\text{-}20)$$

Knowing the values of S′, (H^+), and K_2', enables the prediction of the solubility of CaOx in any given solution. In dI water, the solubility of CaOx rises notably when the pH of solution is less than or equal to 4 and decreases from pH = 5 to pH = 10. It was observed that dI water did not have notable impact on COM crystal dissolution above pH=4. [33] In the low pH region, the existence of [Ox^{2-}] is almost zero. Thus, CaOx dissolution capacity increases in an extremely acidic medium and is reduced in a highly basic solution.

3.3 COM dissolution results

3.3.1 COM dissolution in dI water

The dissolution of COM crystals in this study was evaluated by monitoring the spatial change in size of COM crystals within approximately one hour by image-assisted microscopic process. A graph of the COM dissolution times for dI water at various pH values is shown in Figure 13. It shows the ability of water to dissolve COM crystals increases as the pH decreases. At pH values of 6 or more, very little dissolution was observed during the dissolution monitoring time (72 minutes). The experimental results reported in this study confirm previous results published on COM crystal dissolution in dI water; specifically, after pH=5 there is a significant increase in COM dissolution time. [33, 79, 81-82] In general, previous studies and the present research show that dI water is ineffective as a solution for dissolving COM crystals at pH values of 6 or more.

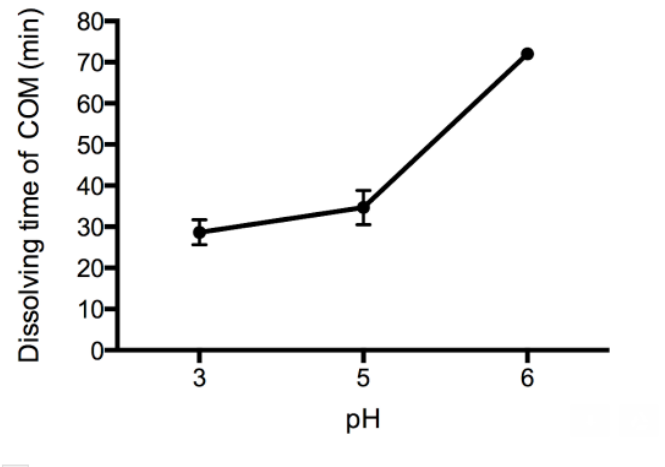

Figure 13. COM dissolution times in water as a function of solution pH. At pH=6, there was no significant COM dissolution. Therefore, the time shown at pH=6 is the time the experiment was stopped.

Figure 14. Images of crystals being irrigated with water solutions that have specific solution pH values. All scale bars are 10 µm.

3.3.2 COM dissolution in sodium acetate trihydrate and sodium formate solutions

At pH=3, the acetate and formate solutions explored are able to dissolve COM salts better than at pH=5 (Figure 15). This increase in dissolution time confirms the conclusion reported by Verplaeste et al. related to the impact of chelating agents on dissolution of COM crystals with decreasing pH. [82] It is observed that dI water, acetate, and formate solutions all had less ability to dissolve COM salts as the solution pH was raised. However, at pH=7, the acetate curve reversed this tendency, showing a decrease in the time needed to dissolve COM crystals. By contrast, while the acetate solution needed less time to dissolve the COM crystals, the formate solution required almost double the time to dissolve COM crystals at pH=7 compared to pH=5. This formate

species trend corroborated the result reported by McComas about the effect of pH on the solubility of calcium oxalate. [80] They found that when the value of pH increases, the COM dissolution capability of the formate ligand decreases. The reason for the decrease in the dissolution between pH values of 5 and 7 is currently unclear.

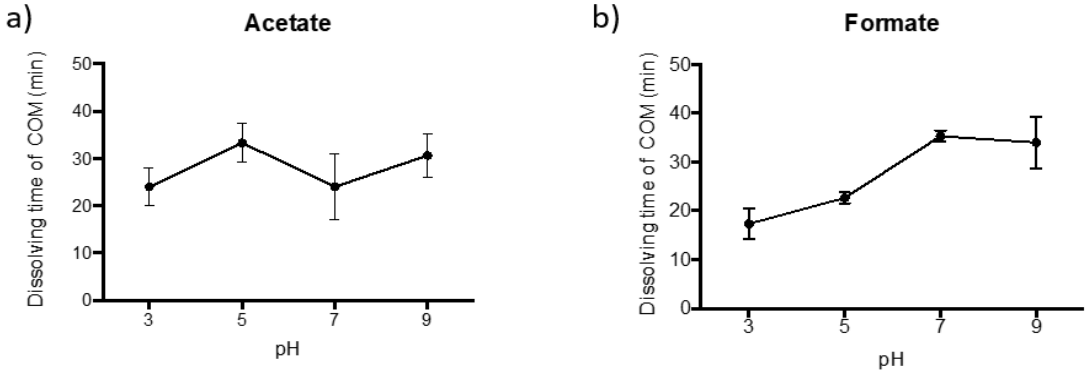

Figure 15. COM dissolution times as a function of solution pH using sodium acetate trihydrate and sodium formate. The error bar shows the range between the reported value and the true values obtained in this study. Each experiment was repeated three times.

At a pH solution pH of 9, acetate showed an increase in time needed for dissolution, while formate exhibited a similar time needed for dissolution compared to when pH=7. The images of COM crystal dissolution at pH=3 and pH=9 are shown in Figure 16. Similar dissolution images at pH=5 and pH= 7 are reported in Figure B.27 (see Appendix).

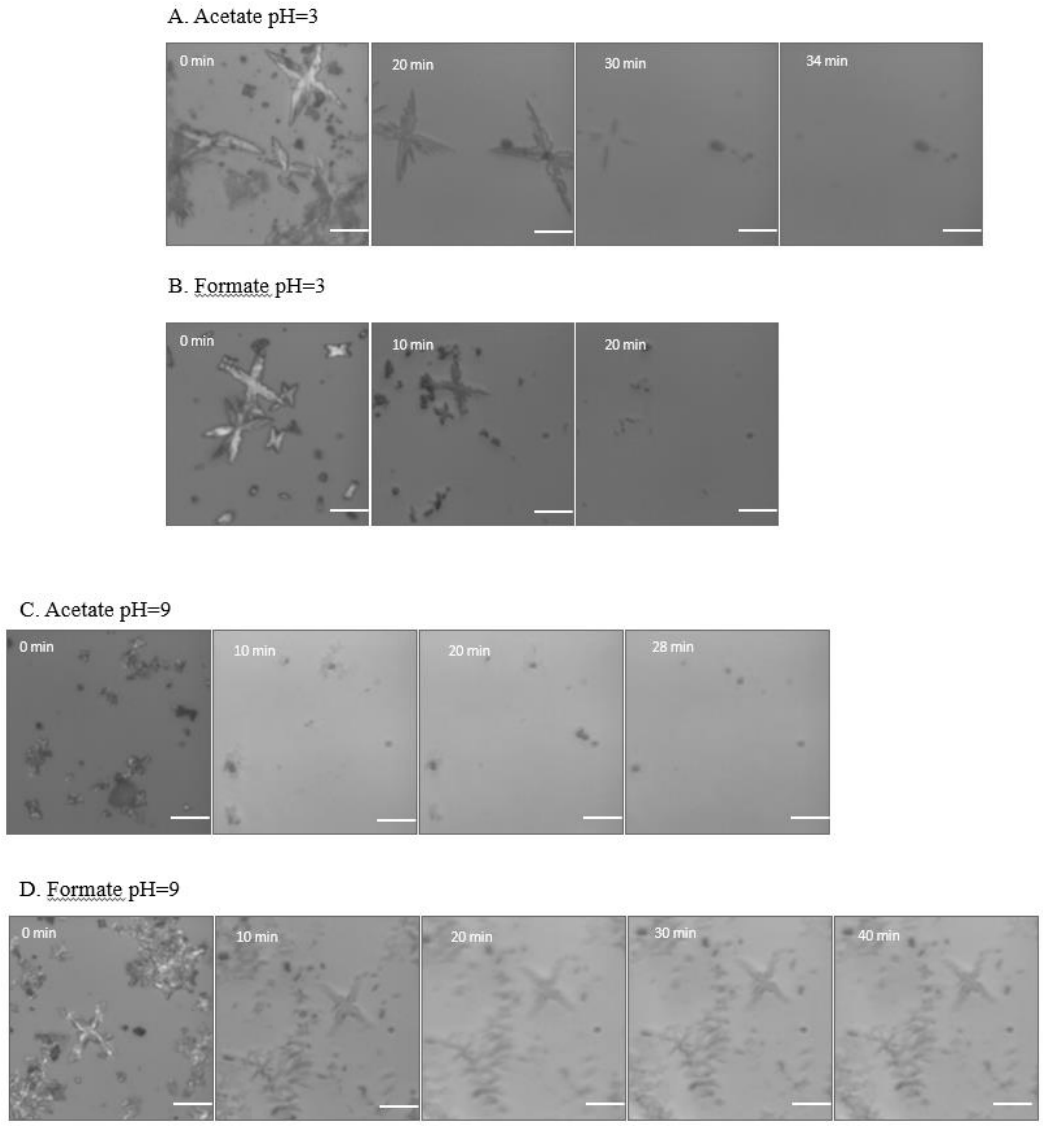

Figure 16. Images of crystals being irrigated with solutions of sodium acetate trihydrate (A, C) and sodium formate (B, D) that have specific solution pH values. All scale bars are 10 µm.

3.3.3 COM dissolution in succinate disodium and malate disodium solutions

At pH= 3, succinate disodium and malate disodium solutions had better ability to dissolve COM crystals than when the pH value was 5. Whereas malate decreased its efficiency in dissolving COM crystals when pH was increased from 5 to 7, succinate by

contrast showed a decrease in dissolution ability when the solution pH was raised from 5 to 7.

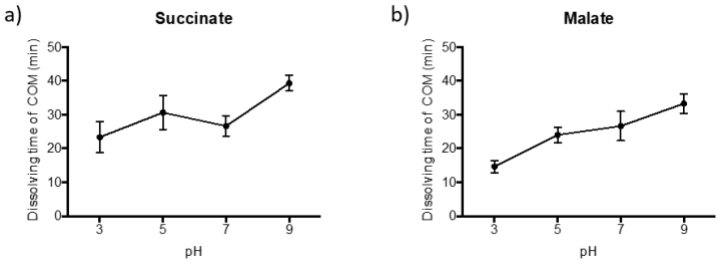

Figure 17. COM dissolution times as a function of solution pH using succinate disodium and malate disodium.

This succinate species trend reversed after pH=7 showing the resistance of COM crystals to dissolution at pH= 9. In general, malate solution showed an increase in the dissolution time needed from pH=3 to pH=9 (Figure 17). The images of COM crystal dissolution at pH=3 and pH=9 are shown in Figure 18. Similar dissolution images at pH=5 and pH= 7 are reported in Figure B.28 (see Appendix).

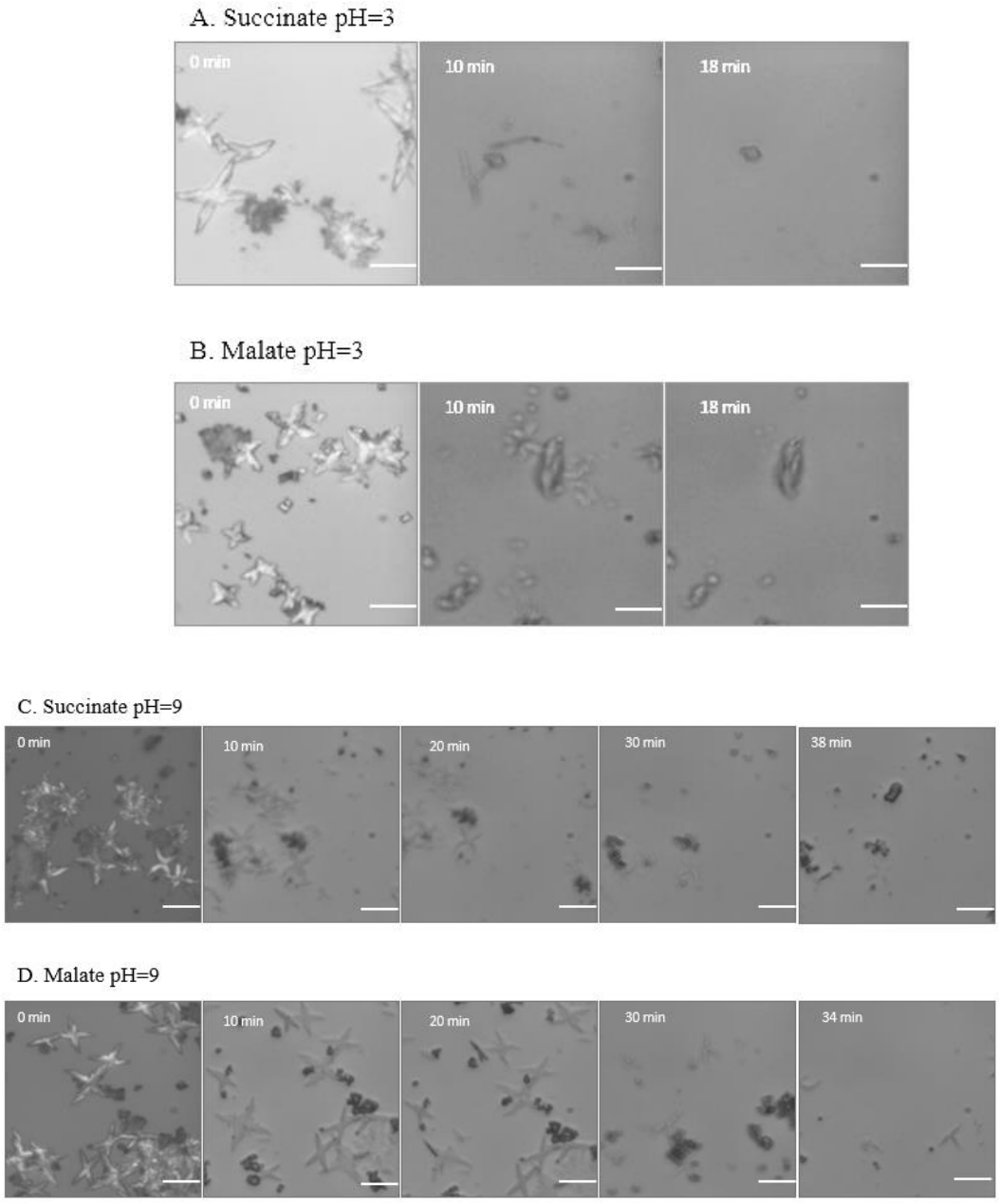

Figure 18. Images of crystals being irrigated with solutions of succinate disodium (A, C) and malate disodium (B, D) that have specific solution pH values. All scale bars are 10 µm.

3.3.4 COM dissolution in sodium citrate dihydrate and potassium hydroxycitrate tribasic monohydrate solutions

At pH below 5, both citrate and hydroxycitrate have a limited effect on COM crystal dissolution capabilities, compared to when pH=7 and 9. At pH=7, citrate clearly shows a substantial decline in the amount of time needed, from 30 min to approximately 15 min compared to the time needed at pH=5. In the pH range from 5-7, citrate has been reported to be a good chelating-agent for Ca^{2+}. The results shown here corroborate those found in the literature. [58, 83] For hydroxycitrate, a similar pattern is observed in the pH range 7 to 9. In the pH range 7 to 9, citrate slowed down its efficiency to dissolve COM crystals while hydroxycitrate increased its dissolution effectiveness, thereby reducing the amount of time required to dissolve COM crystals.

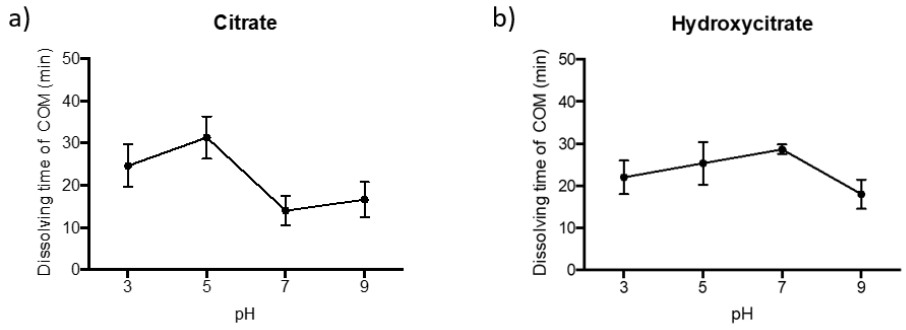

Figure 19. COM crystal dissolution times as a function of solution pH using sodium citrate dihydrate and potassium hydroxycitrate tribasic monohydrate.

The reason why citrate became less efficient than hydroxycitrate could be the presence of an extra hydroxyl group (-OH) on hydroxycitrate ion. This presence of an extra functional group perhaps produces a competitive action on Ca^{2+} by increasing the chelating effect of hydroxycitrate when the alkalinity of solution increases.[34] More

studies are needed to elucidate the real reason why citrate lost the capability to dissolve COM crystals at pH=9.

The images of COM crystal dissolution at pH=3 and pH=9 are shown in Figure 20. Similar dissolution images at pH=5 and pH= 7 are reported in Figure B.29 (see Appendix).

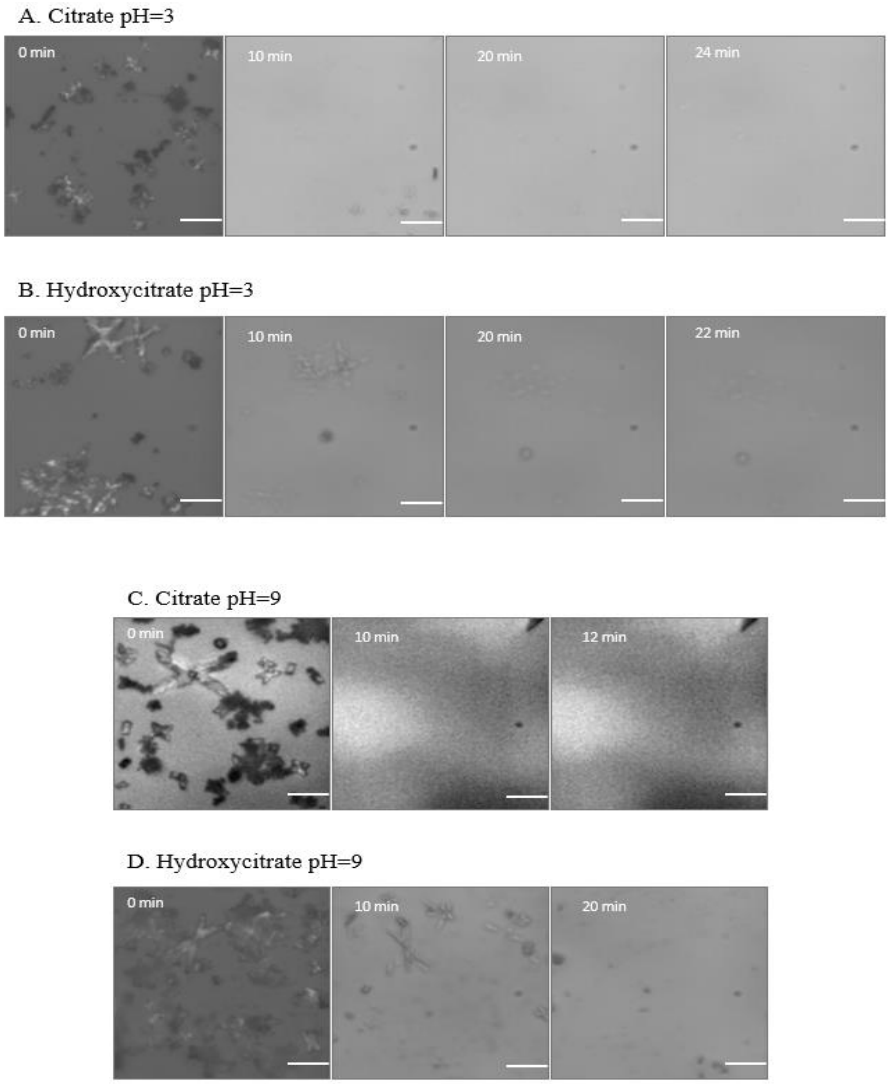

Figure 20. Images of crystals being irrigated with solutions of sodium citrate dihydrate (A, C) and potassium hydroxycitrate tribasic monohydrate (B, D) that have specific solution pH values. All scale bars are 10 µm.

3.3.5 COM dissolution in EDTA and H_4CBUT solutions

Figure 21 illustrates how EDTA and H_4CBUT impacted COM crystals inside a microfluidic device. Both EDTA and H_4CBUT showed a strong effect on dissolving COM salts. At pH 3, EDTA appeared to have a limited effect on the dissolution of COM crystals compared to H_4CBUT and confirmed the conclusion reported by Verplaeste et al. related to the impact of chelating agents on dissolution of COM crystals with decreasing pH. [82] By contrast, the dissolution capabilities of H_4CBUT on COM crystals was relatively constant at pH=3 to pH=5 and the dissolution capability increases at pH=7. The EDTA data show a consistent declining trend in the pH range 5 to 9; implying a substantial decrease in dissolution time for COM crystals. This result corroborates past findings in the literature. [33, 36-37]

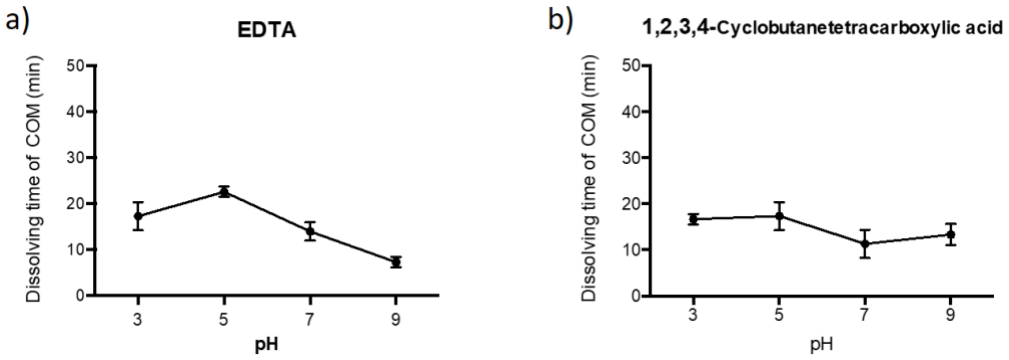

Figure 21. COM dissolution times as a function of solution pH using EDTA and H_4CBUT.

Based on the times determined for EDTA and H_4CBUT, it is obvious that calcium ion is binding to chelating agents. [58, 76, 84-85] The images of COM crystal dissolution at pH=3 and pH=9 are shown in Figure 22. Similar dissolution images at pH=5 and pH= 7 are reported in Figure B.30 (see Appendix).

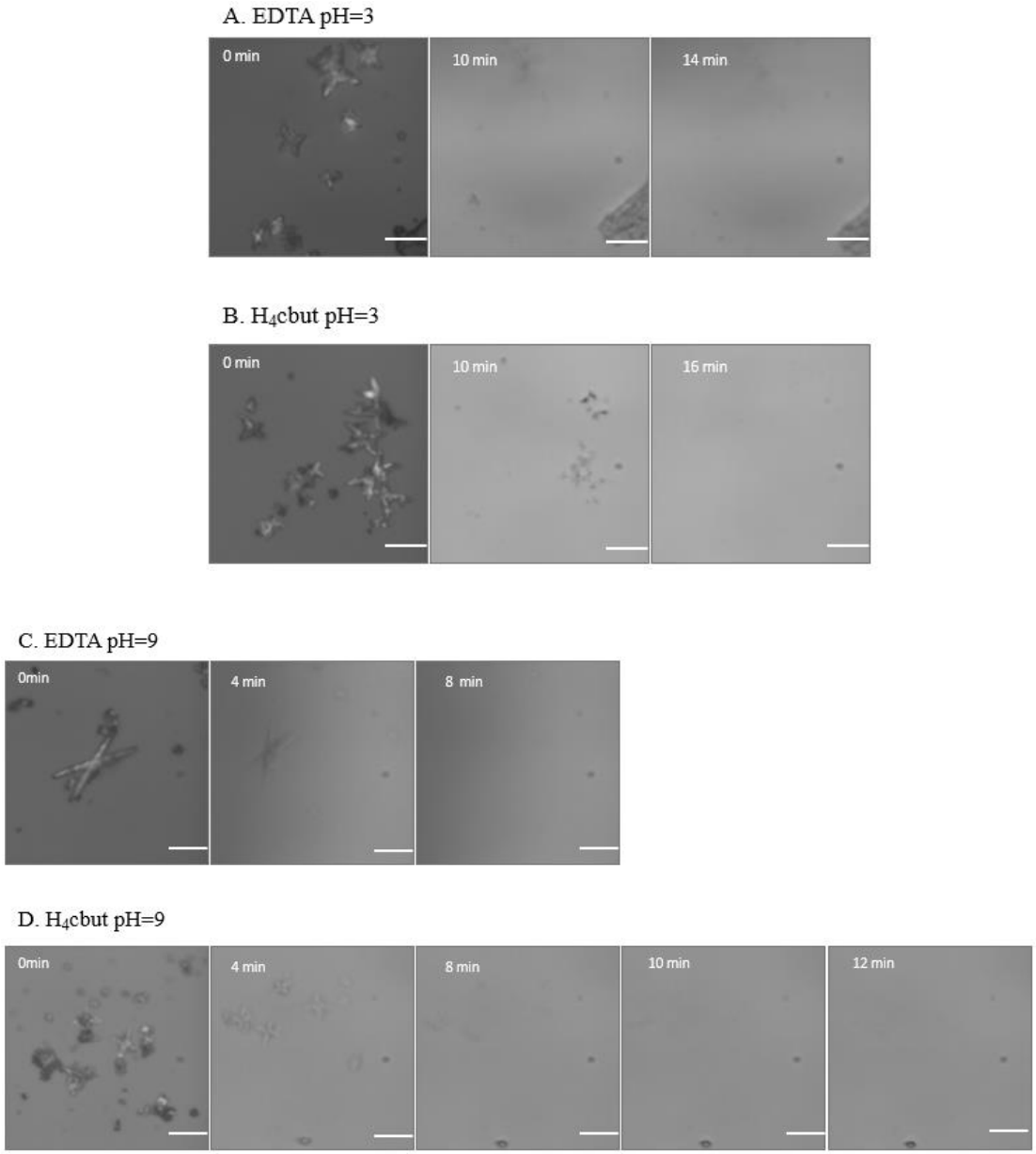

Figure 22. Images of crystals being irrigated with solutions of EDTA (A, C) and H_4CBUT (B, D) that have specific solution pH values. All scale bars are 10 μm.

In the literature, three different opinions have emerged related to the effect of pH on the dissolution of COM crystals. One conclusion is that increasing the solution pH value decreases the dissolution time for COM crystals, [82, 86] while another conclusion is that COM crystal dissolution time increases as solution pH increases. [82, 87-89] Finally,

another opinion is that solution pH has no effect on COM crystal dissolution. [33] It is important to mention that the experimental conditions used in all of these previous studies differed from one group to another. For example, some solutions included sodium chloride, citrate, hydroxycitrate, creatine, urea, artificial urine, and other constituents differing in composition and concentration. Considering the results shown in Figure 23,

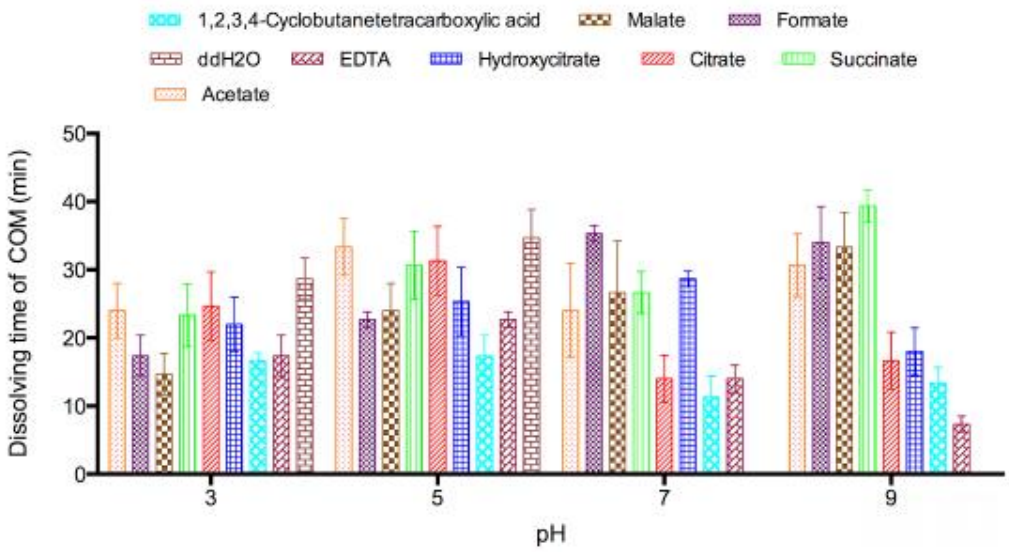

Figure 23. COM dissolution times as a function of solution pH using dI water, acetate trihydrate, sodium formate, succinate disodium, malate disodium, sodium citrate dihydrate, potassium hydroxycitrate tribasic monohydrate, H_4CBUT, and EDTA. ddH_2O means deionized water.

there appears to be no direct correlation between acid type and COM dissolution capability. Each specific dissolution agent shows differing characteristics with respect to solution pH value. The results obtained here suggest the effect of pH is generally specific

to each chelating or dissolution agent.

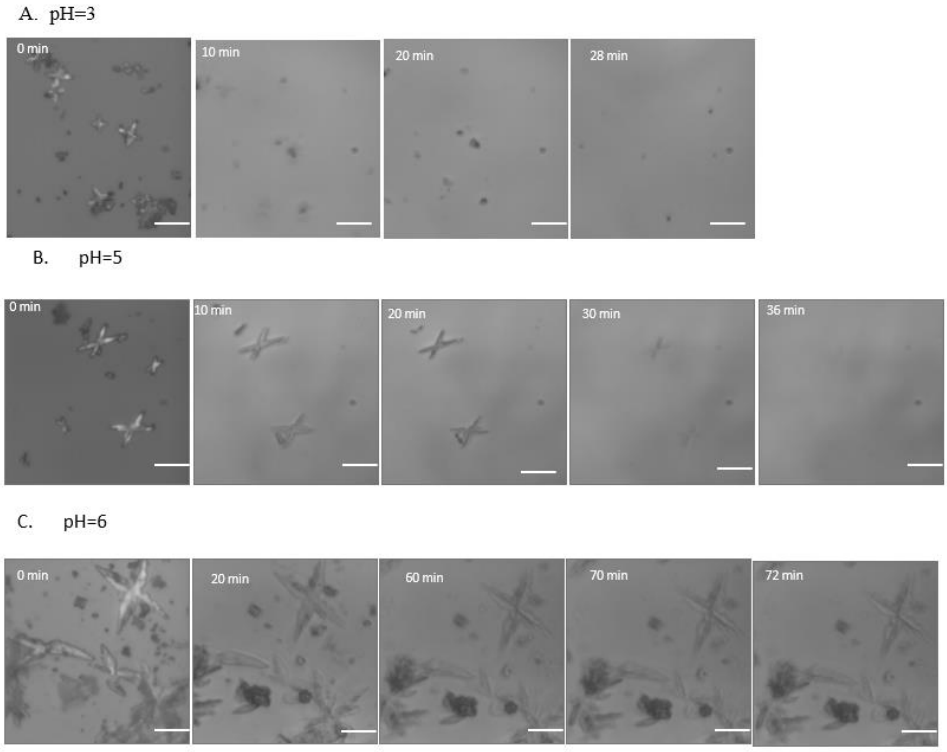

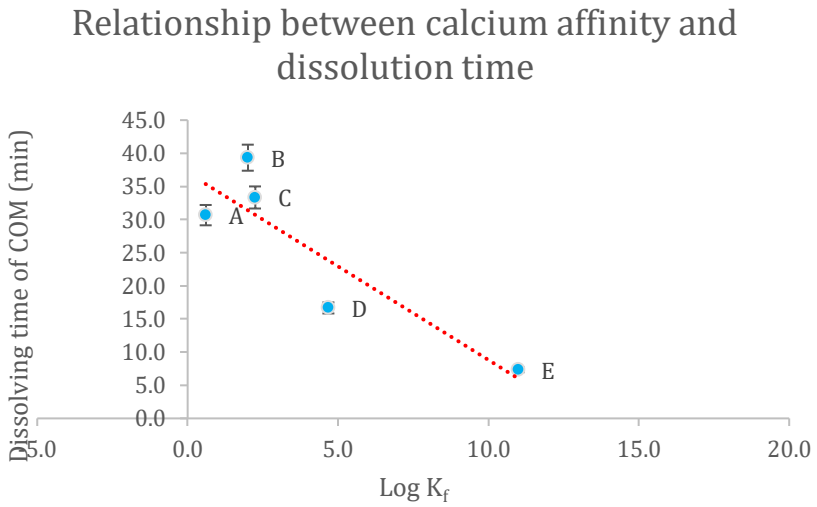

Figure 24. Correlation between COM dissolution time and affinity for calcium ion. A, acetate trihydrate; B, succinate disodium; C, malate disodium; D, sodium citrate dihydrate; E, EDTA. The values for the stability constant (k_f) were obtained from Reference 90.

Figure 24 shows the relationship between the dissolution times of selected dissolution agents fully deprotonated (A, acetate trihydrate; B, succinate disodium; C, malate disodium; D, sodium citrate dihydrate; E, EDTA) on COM crystals at the concentration of 5 mM and the capability that they have to bind to the calcium ion (expressed by the formation constant K_f). Log K_f defines the logarithm of the overall cumulative formation constant for calcium complexes with a specific organic ligand. [90] EDTA and sodium citrate dehydrate are shown to be good dissolution agents in equilibrium with the COM crystals as shown by the relationship between dissolution time of each specific compound plotted and their respective formation constant K_f (Figure 24). Because the stability constant for three out of the eight carboxylic acid used in this study could not be found, these acids were not included in Figure 24.

Summary

This study successfully determined the COM crystal dissolution activity of dI water, acetate trihydrate, sodium formate, succinate disodium, malate disodium, sodium citrate dihydrate, potassium hydroxicitrate tribasic monohydrate, H_4CBUT, and EDTA. At pH solution of 5, the dissolution capability of each dissolution agent examined were: dI water < acetate trihydrate < sodium citrate dihydrate < succinate disodium < potassium hydroxycitrate tribasic monhydrate < sodium formate < H_4CBUT < EDTA < malate disodium. For all of dissolution agents used in this study the dissolution time decreases when the pH solution reduces from 5 to 3. At pH 7, sodium citrate dihydrate, acetate trihydrate, EDTA, H_4CBUT, and succinate disodium required less time (compared to when the solution pH was 5) to dissolve the COM crystals. By contrast, the dissolution time increased when the solution pH was increased from 5 to 7 for dI water, malate disodium, and sodium formate. At pH 9, dI water, succinate dissodium, malate disodium, and acetate trihydrate show an increase in the amount of time required to dissolve COM crystals. By contrast, EDTA, sodium formate, and potassium hydroxycitrate tribasic decrease the dissolution time of COM salts as pH is increased from 7 to 9. This study observed a correlation between dissolution time of specific dissolution agent and formation constant. When the chelating agent has at least three carboxylic functional groups, its formation constant is high and the chelating agent has more capability to dissolve COM crystals as indicated by the linear correlation shown in Figure 24 (i,e. sodium citrate dihydrate and EDTA had more affinity by chelating calcium ions present at 5 mM in equilibrium with COM solids).

Chapter 4 Future Directions

In this study, COM dissolution via a microfluidic device was performed using a series of carboxylic acids as dissolution agents. The experiments described in the previous chapter demonstrate that while the dissolution ability of some additives improves as the solution pH increases, the dissolution capabilities of other additives follows an opposite trend. Furthermore, for some dissolution agents used in this study, solution pH had no significant impact on dissolution activity. Thus, it is not surprising that various groups appear to come to different conclusions with respect to how solution pH influences COM dissolution. Currently, there is no reported method of predicting this trend for a particular carboxylic acid agent. This study suggests that as the number of carboxylate groups on the fully deprotonated form of a specific acid increases, it is more likely that an increase in pH will improve the dissolution ability of that acid. This conclusion is not unexpected. The reported complex stability constants of fully deprotonated carboxylic acids generally increase as the number of carboxylate groups increase, [57] and these fully deprotonated species become the dominant species as pH increases. However, this study was limited to approximately 2 members of each acid type. In order to obtain a more representative viewpoint, it would be constructive to include 4-5 members of each acid type.

In the course of this study, several problems arose which need to be considered for similar future work. A limited number of specific solution pH values (4 for each specific acid) were determined to analyze the capability of a specific acid to dissolve the COM crystals. This limited number of specific solution pH values restricted the determination of a more detailed view of the general effect of solution pH on COM crystal dissolution

for each dissolution agent. Increasing the number of specific solution pH values would give a more complete picture of the influence of pH on the dissolution process.

The initial intent of this research was to characterize the pH-dependent COM dissolution abilities of a relatively large (approximately 25) collection of carboxylic acid types (from monoprotic to tetraprotic). In the pH range chosen (pH = 3-10), the plan was to measure the dissolution abilities for each acid at specific pH values (~8 different pH values) and to do triplicates of each experiment. This implies a total of 24 experiments for each acid, or 120 experiments total. In order to complete such a project, it will be beneficial to reduce the time required to collect the experimental data. One solution is to make a device that allows (multiple) experiments to be done at the same time. The main idea is to decrease the overall time needed to repeat or expand the work presented in this study.

Another issue comes from the use of a "flow through" device such as the dissolution device used in this study: the probability of "washing away" the COM crystals instead of dissolving them, i.e., gradually and spatially diminishing the size of COM crystals. Every time this happened in this study, the experiment in progress was stopped and a new test was started. Trapping the crystals under observation so that they cannot move away is a viable solution to this problem. [91] Preliminary experiments done in this study involved microfabricated traps on the crystal collection slides that are used during the crystal synthesis process (Figure 24 a). Unfortunately, crystals flowing out of the microfluidic crystallization device aggregated significantly arround these traps (Figure 24 b). Thus, it was difficult to find isolated trapped crystals that could be monitored during dissolution. To overcome this problem, a possible solution would be to reduce the crystal collection

time, such as by synthesizing and collecting fewer crystals. It is assumed that fewer crystals will lead to less aggregation.

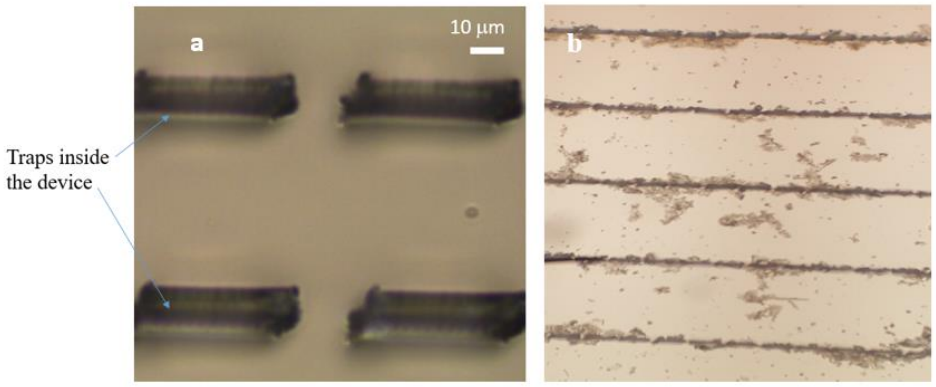

Figure 25. a) Polyacrylate traps on a glass slide. b) Aggregation of COM crystals around the traps.

No COM dissolution times for any simple mixture of two or three carboxylic acids was done in this study. Consequently, this study did not determine the behavior of mixed dissolution agents on COM dissolution. In future study, it would be constructive to characterize the influence of simple mixtures of dissolution agents on COM crystal dissolution.

The experimental approach used in this work did not allow information about how the dissolution agents influence COM dissolution to be gained at a microscopic level. As previously mentioned, the dissolution behavior of solids is generally characterized by three different mechanisms which are transport-controlled, interface-controlled, and mixed-kinetic-controlled. Each of these mechanisms is based on an interfacial step and a mass transport step. The future study can include atomic force microscopy (AFM) to inspect closely and thoroughly the influence of dissolution agents on COM dissolution process at a microscopic level. One approach would be to first collect AFM images of crystals from the crystallization process. Next, these crystals can be irrigated with a

specific dissolution agent solution for a particular amount of time. Finally, AFM images of these crystals can be collected after this irrigation. A comparison between the two sets of AFM images should provide some insights into how the dissolution process is occurring microscopically.

Appendix

A.1 Solid states: crystalline and amorphous

In crystallography, solids are grouped into two categories: crystalline and amorphous. A crystalline solid is a substance whose essential elements possess a well-ordered arrangement. These include sucrose, diamond, and sodium chloride, to name a few. An amorphous solid is a substance whose components do not have a regular well-ordered arrangement. Rubber, glass, polymers, and gels fit in this category. Crystalline solids and amorphous solids have different characteristics. Crystalline solids have a definite and regular geometry, sharp melting points, and a specific heat of fusion. In addition, crystalline solids are stiff and cannot be easily deformed. By contrast, amorphous solids do not have a regular geometry, do not have a sharp melting point, and can be deformed by bending or compression efforts. Amorphous solids are considered cooled liquids or pseudo solids. The physical properties of crystalline solids are anisotropic (varied physical properties in different directions) but amorphous solids are isotropic (varied physical properties are same in all directions. [92-94]

A.2 Crystalline solid

A.2.1 Categories of crystalline solids

Crystalline solids can be categorized into different groups depending upon the type of constituent elements and the sort of attractive forces occurring between the constituent elements of the crystal. There are atomic solids, molecular solids, ionic solids, covalent solids, and metallic solids. Atomic solids have atoms as elemental building blocks. London dispersion forces link their block structures. Most of these atomic solids are crystals of noble gases. In molecular solids, the constituent elements are molecules of

substances packed together by Van der Waals forces (dispersion forces); dry ice and iodine are examples. Dipole-dipole forces (e.g., in solid HCl) and hydrogen bonds (e.g., in HF and solid ammonia) are other attractive forces that can act between the molecules in the solid state. In ionic solids, the component elements are ions of different charges. The forces attracting the ions of opposite charges are ionic bonds (e.g., in CsCl, ZnS, and CaF_2). In covalent solids, the component elements are atoms of the same or different elements attached to each other by a covalent bond network (e.g. in diamond, quartz, and silicon). Finally, metallic solids, of which the constituent particles are metal atoms, are linked by metallic bonds such as Cu, Fe, and Zn. [92]

A.2.2 Polymorphism of crystalline solid

Crystalline solids can also exist in two or more forms called polymorphs. Polymorphs have distinct structures with the same chemical constitution but different internal crystal arrangements. [95] Polymorphism can be characterized into two types. The first type is called packing or oriented polymorphism. This type of polymorphism exists as a consequence of rigid molecules adopting identical conformation packed in distinct ways. For example, acetaminophen, a crystalline substance, has the same conformation with different systems: orthorhombic (space group: *Pbca*) and monoclinic (space group: $P2_1/n$). [96]

The second category is conformational polymorphism. This type of polymorphism occurs when flexible molecules deform, adopting different conformations packed in different forms of crystals. For example, Spiperone, a typical antipsychotic and pertaining to butyrophenone chemical class, has two distinct conformations (space group: $P2_1/a$ and $P2_1/c$) packed in the same monoclinic system. [96]

Each polymorph has a distinct X-Ray diffraction pattern because each polymorph has a unique atomic arrangement and crystal structure. In addition, crystalline polymorphs have distinct physical and chemical characteristics such as different melting points, habits, flow, density, and solubility. [95, 97] Furthermore, ability to interchange from one polymorph to another defines their characteristic as enantiotropic (reversible change of a crystal between different phases that take place when heated above a transition point temperature) or monotropic (polymorph which is irreversible) molecules which can be distinguished one from another by their heat of fusion. [94] There are also other types of crystalline solids called solvates or pseudopolymorphs defined as organic compounds that contain a solvent of crystallization other than water. [95] In pseudopolymorphism, the different categories of crystal are consequences of hydration or solvation. [98] If water is the solvent, the terminology "hydrate" is used. As defined by Vippagunta et al., "a hydrated crystal is one that contains water within its structure and reported in its formula". When the solvent in a solvate is eliminated and the crystal conserves the structure of a solvate, it is known as a desolvated solvate. [98]

A.3 Crystalline state: fundamental concepts

According to the International Union of Crystallography (IUCr), a substance is called a crystal if it presents a sharp diffraction structure or "essentially discrete diffraction diagram". [99] This definition "goes beyond three-dimensional periodicity to include quasicrystals and other unexpected structures that might be discovered". [100] As mentioned above, a common technique used to determine crystal arrangement is X-ray crystallography, a method of diffraction analysis, that reveals the interior structure of the atoms in the crystal, and thus characterizes the bond angles and interatomic spaces. A

basic unit (unit cell) defines the crystal structure. The unit cell refers to a set of atoms, which are linked together in a specific geometrical manner.

In crystallography, the descriptions of planes, faces, set of faces, volumes, axes, and angles are important to characterize the unit cell of a crystal. The coordinates *a*, *b* and *c* possess an exact physical form outlined by the translational vectors $\vec{a}$, $\vec{b}$, and $\vec{c}$ giving a perceptible volume *V* that includes the essential molecules or atoms that form the crystal unit structure. [101] In addition, *a, b,* and *c* characterize the lengths of cell edges, and the symbols α, β, and γ are the values of the angles between these vectors of the cell edges, as shown in Figure A. 25. Moreover, the atomic locations inside the unit cell are represented by the set of atomic positions X_i, Y_i, and Z_i. The atomic positions are calculated from a designated reference lattice point, a location in the unit cell with high probability of finding an ion or an atom. [102]

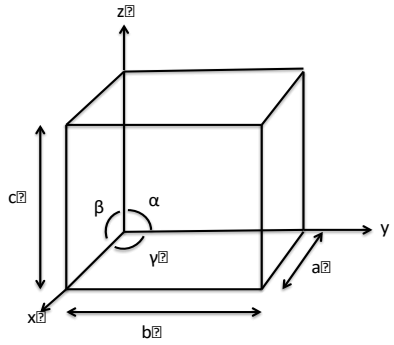

Figure A.26 Axes, unit cell dimension, and angles for a general unit cell.

In crystallography, there are three entities (*l, m, n*) called Miller index notations, which represent the vectors and planes in a crystal lattice. For example, (100) symbolizes the Miller index of a plane in a cubic unit cell. By definition, the syntax (*l, m, n*) indicates the plane that connects three points *a*/*l*, *b*/*m*, and *c*/*n* or some multiple of them. Thus, the Miller indices correspond to the inverses of the intersections of a plane formed by the

three points and the unit cell. Indices zero (0) means that the planes do not cross the axis. The values of Miller indices are not decimals and negative indices are represented with a bar on the top of the indices as in $(1,\bar{1}, 2)$. [102]

Fourteen different lattices, called Bravais lattices, can be formed in a three-dimensional representation of lattice points. Bravais lattices can be subdivided by symmetry and centering into seven lattice systems: isometric or cubic, tetragonal, orthorhombic, monoclinic, triclinic, hexagonal, and rhombohedral. Bravais lattices can be categorized into four different sorts. The first category is represented by a primitive lattice (P) and rhombohedral lattice (R) that only have lattice points at each corner of the three-dimensional unit cell. The second type is the body-centered lattice for "Innenzentrierte" lattices (I). In addition to having lattice points at each corner of the unit cell, a body-centered lattice has a lattice point at the center of the three-dimensional unit cell. The third variety is the base-centered lattice, represented by A, B, or C faces; additional lattice points are involved at the centers of the opposing unit cell faces for centered lattices. The fourth category is a face-centered lattice (F), which contains additional lattice points at the corners of the unit cell and at either the centers of one pair of faces or the centers of all three pairs of faces. [103] The symmetries restrict the representation of these coordinates and angles in three dimensions as shown in Table 3.

In crystallography, symmetry is applied to characterize all crystals. Symmetry is a precise correlation between parts of a shape with respect to a separated line, plane, or point. Symmetry elements include entities such as Identity (E), Symmetry planes (σ), Inversion center (I), Proper axis (C_n), and Improper axis (S_n). These elements involve operations such as rotation, reflection, and inversion. [104] There are two forms of

symmetry notation: the Schoenflies notation, used to characterize the point group of a crystal lattice, and the Hermann-Mauguin notation, which is able to define the space group. [103]

Lattice System	Unit Cell	14 Bravais Lattices
triclinic	$a \neq b \neq c$; $\alpha \neq \beta \neq \gamma = 90^o$	P
monoclinic	$a \neq b \neq c$; $\alpha = \gamma = 90^o$; $\beta \geq 90^o$	P, C
orthorhombic	$a \neq b \neq c$; $\alpha = \beta = \gamma = 90^o$	F, I, A (B or C)
tetragonal	$a = b \neq c$; $\alpha = \beta = \gamma = 90^o$	P, I
rhombohedral	$a = b = c$; $\alpha = \beta = \gamma \neq 90^o$	R
hexagonal	$a = b \neq c$; $\alpha = \beta = 90^o$; $\gamma = 120^o$	P
cubic	$a=b=c$; $\alpha= \beta = \gamma = 90^o$	P, F, I

Table A.3 Seven lattice systems and their characteristics. [103]

The totality of symmetry elements existing in a molecule composes a “group”, specifically named a point group. It is the expression of the intersection of all the symmetry elements (points, lines, and planes) at a single point. A point group is defined as a collection of symmetry operations such as rotation and reflection. On the other hand, a space groups refers to the symmetry group of a structure or configuration in three dimensions. In space, a combination of the 32 three dimension (3 D) crystallographic point groups with 14 Bravais lattices (associated with one of the 7 lattice systems) generates a totality of 230 possible space groups entirely characterizing all probable

crystal symmetries. [105] The space group can be classified into 7 crystal systems (Table 4) each possessing specific symmetry operations. Moreover, each crystal system correlates with one of six different crystal families. The crystal system includes hexagonal, trigonal, monoclinic, orthorhombic, tetragonal, triclinic, and cubic systems (Figure 26). [103-104, 106]

There are more than ten methods to describe a space group. The "International short symbol" is the one most generally used in crystallography. This method includes a set of four signs. For example, quartz is a trigonal crystal included in the space group $P3_121$. The symbol *P* refers to primitive unit cell, 3_1 signifies the symmetry along the major axis (*c* axis in trigonal crystal), *2* refers to the symmetry along axes of less significance (*a* or *b* in trigonal crystal) and 1 shows the symmetry in the remaining axis. [104]

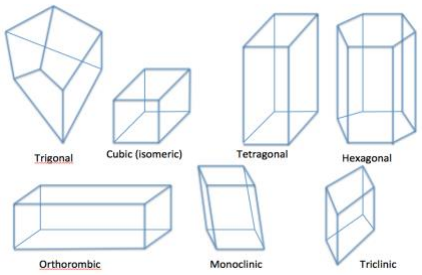

Figure A.27 The seven crystal system forms. [103]

Crystal System	Unit Cell	Symmetry
Trigonal	$a^1 = a^2 = a^3 \neq c$; $\alpha = \beta = \gamma = 120^o$	1 3-fold axis of rotation
Monoclinic	$a \neq b \neq c$; $\alpha = \gamma = 90^o$; $\beta \geq 90^o$	1 2-fold axis of rotation
Orthorhombic	$a \neq b \neq c$; $\alpha = \beta = \gamma = 90^o$	3 2-fold axis of rotation
Tetragonal	$a = b \neq c$; $\alpha = \beta = \gamma = 90^o$	1 4-fold axis of rotation
Triclinic	$a \neq b \neq c$; $\alpha \neq \beta \neq \gamma \neq 90^o$	No axis of symmetry
Hexagonal	$a^1 = a^2 = a^3 \neq c$; $\alpha = \beta = \gamma = 120^o$	1 6-fold axis of rotation
Cubic	$a=b=c$; $\alpha = \beta = \gamma = 90^o$	4 3-fold axis of rotation

Table A.4 Seven crystal system and their characteristics. [103]

B.1 Images of COM crystal being irrigated with sodium acetate trihydrate or sodium formate solutions at pH=5 and pH=7

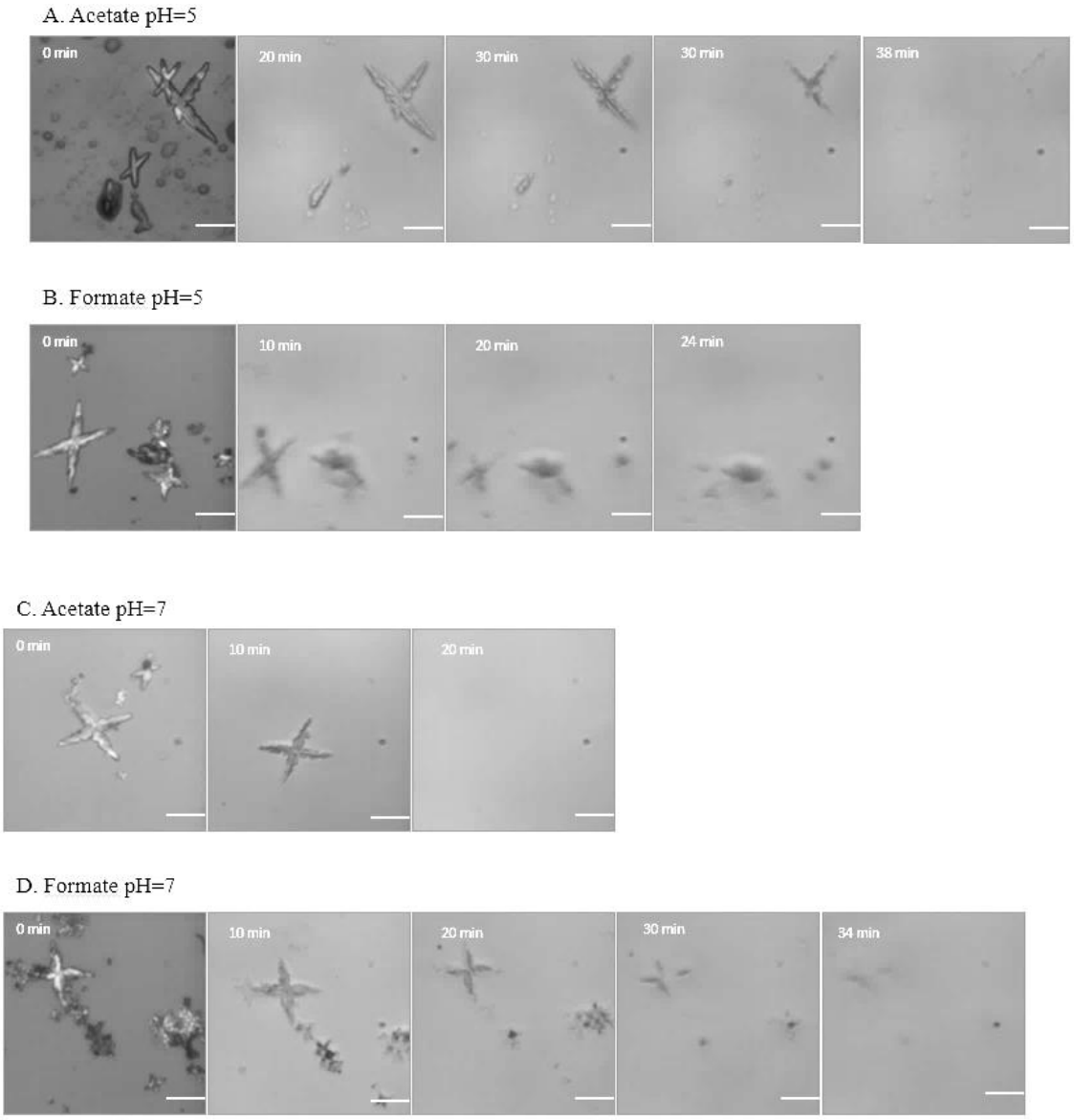

Figure B.28 Images of crystals being irrigated with solutions of sodium acetate trihydrate (A, C) and sodium formate (B, D) that have specific solution pH values. All scale bars are 10 μm.

B.2 Images of COM crystal being irrigated with succinate disodium or malate disodium solutions at pH=5 and pH=7

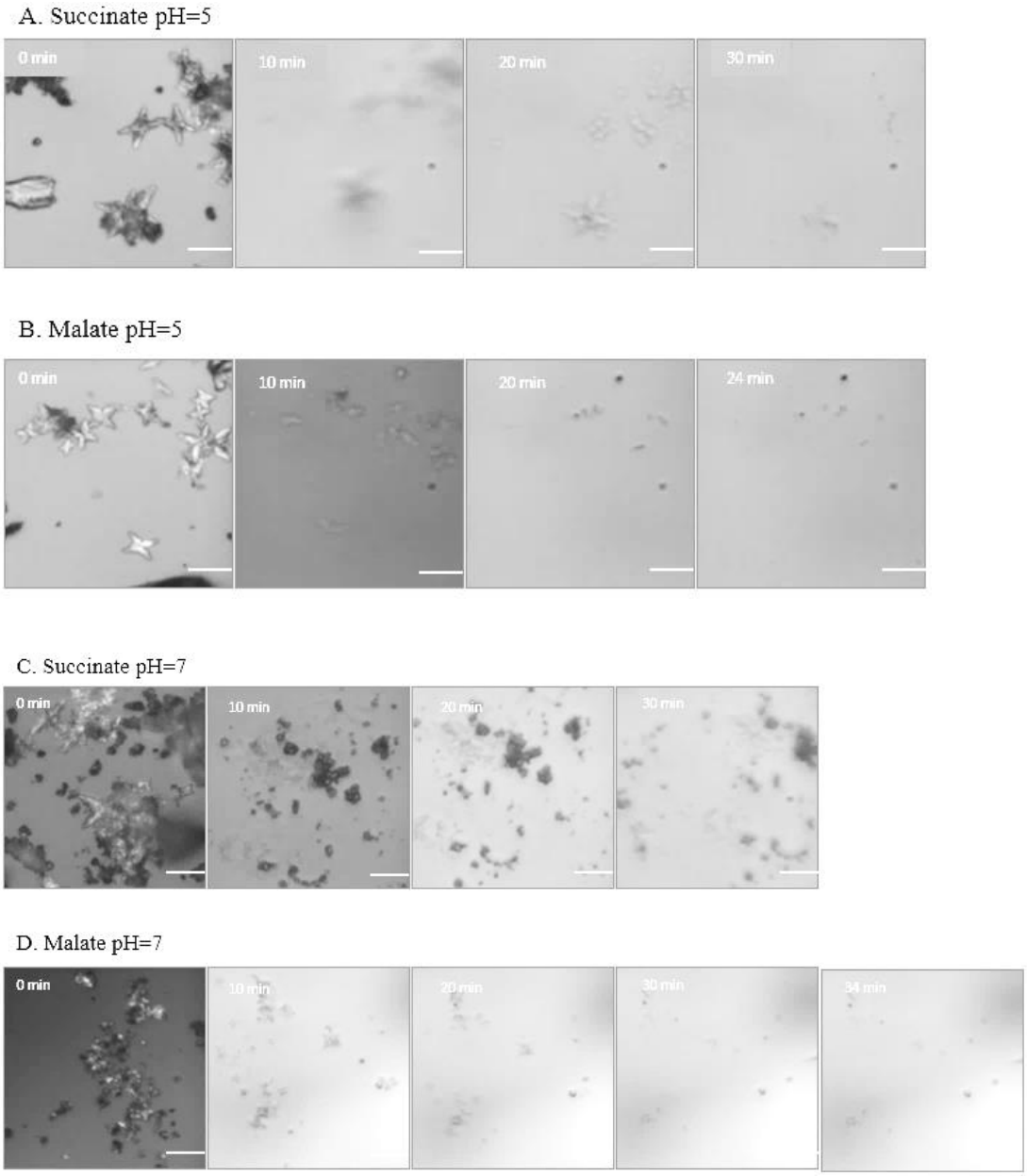

Figure B.29 Images of crystals being irrigated with solution of succinate disodium (A, C) and malate disodium (B, D) that have specific solution pH values. All scale bars are 10 μm.

B.3 Images of COM crystal being irrigated with sodium citrate dihydrate or potassium hydroxycitrate tribasic monohydrate solution at pH=5 and pH=7

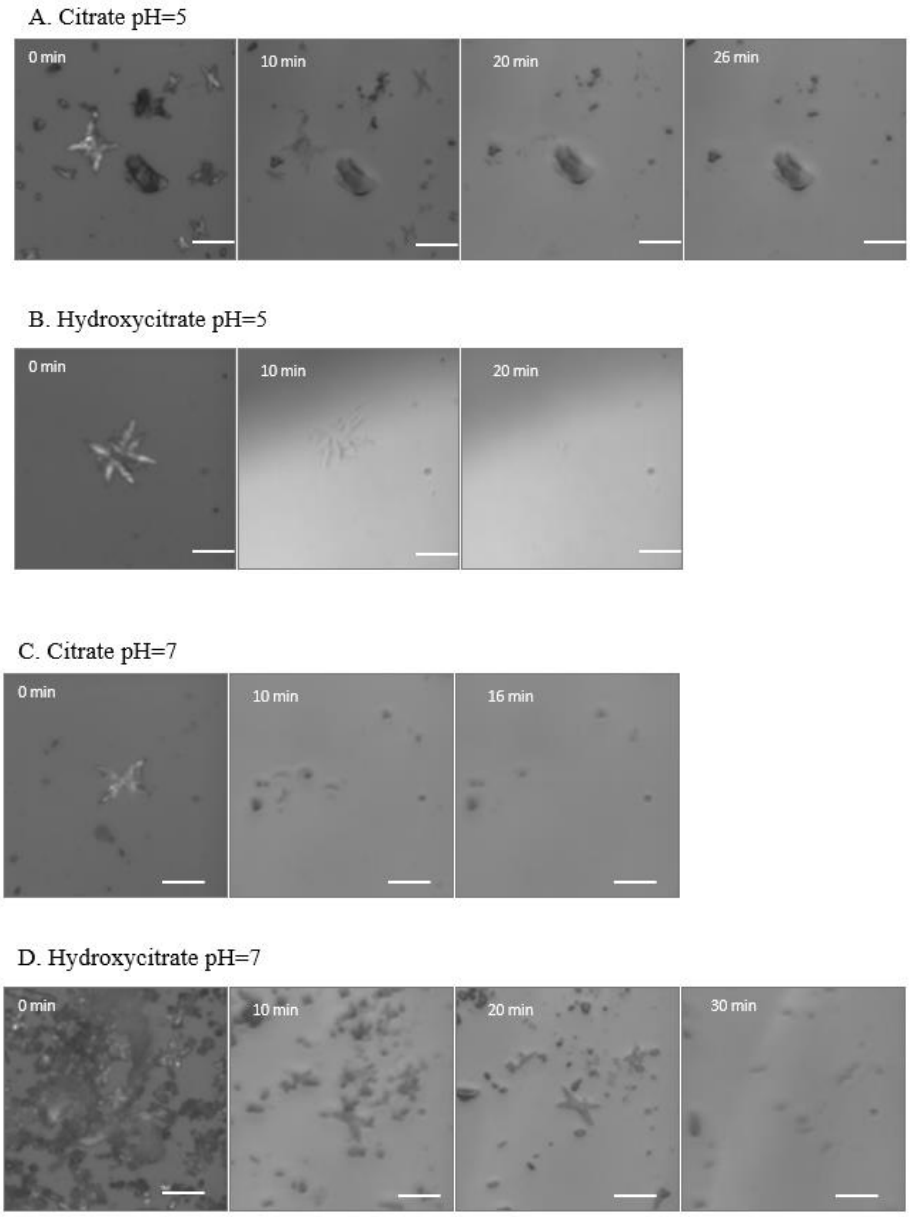

Figure B.30 Images of crystals being irrigated with solutions of sodium citrate dihydrate (A, C) and potassium hydroxycitrate tribasic monohydrate (B, D) that have specific solution pH values. All scale bars are 10 µm.

B.4 Images of COM crystal being irrigated with EDTA or H4CBUT solutions at pH=5 and pH=7

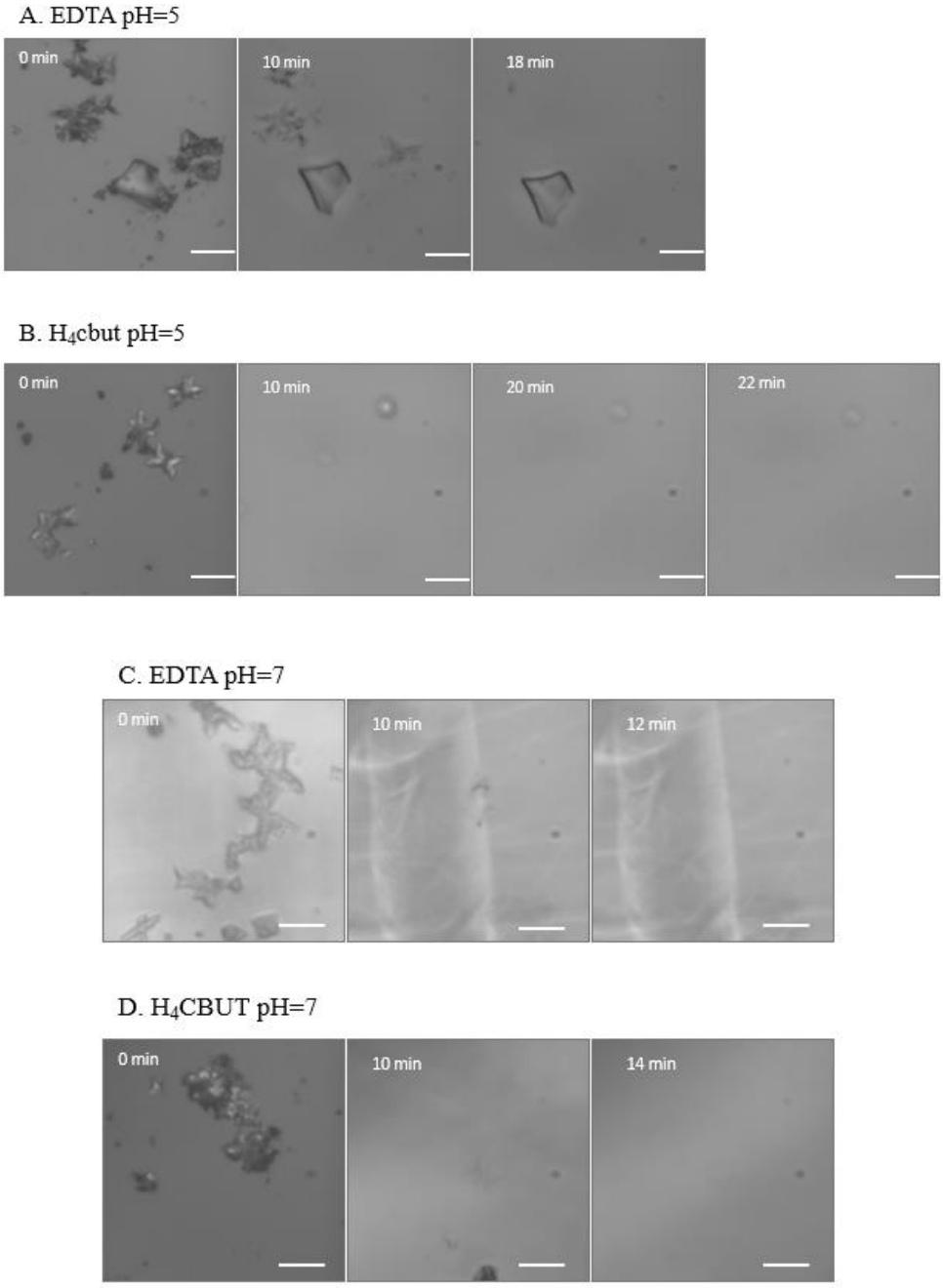

Figure B.31 Images of crystals being irrigated with solutions of EDTA (A, C) and H_4CBUT (B, D) that have specific solution pH values. All scale bars are 10 µm.

References:

1. Franceschi, V. R., & Nakata, P. A., Calcium oxalate in plants: formation and function. *Annual Review of Plant Biology* **2005,** *56*, 41-71.

2. Brečević, L., Škrtić, D., & Garside, J., Transformation of calcium oxalate hydrates. *Journal of Crystal Growth* **1986,** *74* (2), 399-408.

3. Gorostiza, P., & Isacoff, E. Y., Optical switches for remote and noninvasive control of cell signaling. *Science* **2008,** *322* (5900), 395-399.

4. Coe, F. L., Evan A., Worcester, E., Kidney stone disease. *Journal of Clinical Investigation* **2005,** *115* (10), 2598.

5. William, O. S. D., Effect of calcium and magnesium ions on calcium oxalate formation in sugar solutions. *Industrial & Engineering Chemistry Research* **2006,** *45* (2), 642-7.

6. Pinna, D., Fungal physiology and the formation of calcium oxalate films on stone monuments. *Aerobiologia* **1993,** *9* (2-3), 157-167.

7. Caneva, G., Ecological approach to the genesis of calcium oxalate patinas on stone monuments. *Aerobiologia* **1993,** *9* (2-3), 149-156.

8. Saigal, C. S., Joyce, G., & Timilsina, A. R., Urologic Diseases in America Project: direct and indirect costs of nephrolithiasis in an employed population: opportunity for disease management? *Kidney International* **2005,** *68* (4), 1808-1814.

9. Baldwin, H., An experimental study of oxaluria, with special reference to its fermentative origin. *Journal of Experimental Medicine* **1900,** *5* (1), 27-46.

10. Worcester, E. M., & Coe, F.L., Nephrolithiasis. *Primary Care: Clininics in Office Practice* **2008,** *35* (2), 369-91.

11. Sinha, M. R., Dev, A., Prasad, A., Ghosh, M., & Tagore, R. N., Experimental study of solubility of urinary stones in juice of Chikku (Achras zapota) fruit. *Journal of Chemical and Pharmaceutical Research* **2011,** *3* (1), 231-237.

12. Meschi, T., Maggiore, U., Fiaccadori, E., Schianchi, T., Bosi, S., Adorni, G., Ridolo, E., Guerra, A., Allegri, F., Novarini, A., & Borghi, L., The effect of fruits and vegetables on urinary stone risk factors. *Kidney International* **2004,** *66* (6), 2402-2410.

13. Odvina, C. V., Comparative value of orange juice versus lemonade in reducing stone-forming risk. *Clinical Journal of the American Society of Nephrology* **2006,** *1* (6), 1269-1274.

14. Girasa, W., & De Wispelaere, M., Polyaspartate, a new alternative for the conditioning of cooling water. *In 14th International Conference on the Properties of Water and Steam, Kyoto, Japan* **2004,** *49*.

15. Quan, Z., Chen, Y., Wang, X., Shi, C., Liu, Y., & Ma, C., Experimental study on scale inhibition performance of a green scale inhibitor polyaspartic acid. *Science in China Series B: Chemistry* **2008,** *51* (7), 695-699.

16. Zuhl, R. W., & Amjad, Z., Scale and deposit control polymers for industrial water treatment. *Science and Technology of Industrial Water Treatment* **2010,** *6*, 81-103.

17. Cuajungco, M. P., Faget, K. Y., Huang, X., Tanzi, R. E., & Bush, A. I., Metal chelation as a potential therapy for Alzheimer's disease. *Annals of the New York Academy of Sciences* **2000,** *920* (1), 292-304.

18. House, E., Collingwood, J., Khan, A., Korchazkina, O., Berthon, G., & Exley, C., Aluminium, iron, zinc and copper influence the in vitro formation of amyloid fibrils of Aβ 42 in a manner which may have consequences for metal chelation therapy in Alzheimer's disease. *Journal of Alzheimer's Disease* **2004,** *6* (3), 291-301.

19. Joshi, H. B., Kumar, P. V. S., & Timoney, A. G., Citric acid (solution R) irrigation in the treatment of refractory infection (struvite) stone disease: is it useful? *European Urology* **2001,** *39* (5), 586-590.

20. Olivieri, N. F., & Brittenham, G. M., Iron-chelating therapy and the treatment of thalassemia. *Blood* **1997,** *89* (3), 739-761.

21. Patel, P. B., & Vadalia, K. R., Effect of chelating biomolecules on solubility of calcium oxalate: An in vitro study. *Journal of Chemical and Pharmaceutical Research* **2011,** *3*, 491-495.

22. Xiang-bo, Z., Zhi-ping W., Jian-min, D., Jian-zhong L., & Bao-liang, M., New chemolysis for urological calcium phosphate calculi - a study in vitro. *BioMed Central* **2005,** *5* (1), 9.

23. Gonzalez, R. D., Whiting, B. M., & Canales, B. K., The history of kidney stone dissolution therapy: 50 years of optimism and frustration with renacidin. *Journal of Endourology* **2012,** *26* (2), 110-118.

24. Fink, H. A., Akornor J.W., Garimella P.S. Mac Donald R., Cutting A., Rutks I.R., Monga M., & Wilt T.J., Diet, fluid, or supplements for secondary prevention of nephrolithiasis: a systematic review and meta-analysis of randomized trials. *European Urology* **2009,** *56* (1), 72-80.

25. Pak, C. Y., Pharmacotherapy of kidney stones. *Expert Opinion on Pharmacotherapy* **2008,** *9* (9), 1509-18.

26. Saso, L., Valentini, G., Leone, M. G., Grippa, E., & Silvestrini, B., Development of an in vitro assay for the screening of substances capable of dissolving calcium oxalate crystals. *Urologia Internationalis* **1998,** *61* (4), 210-214.

27. Ngo, T. C., & Assimos, D. G., Uric acid nephrolithiasis: recent progress and future directions. *Reviews in Urology* **2007,** *9* (1), 17.

28. Heimbach, D., Jacobs D., Muller S. C., & Hesse, A., Improving cystine stone therapy: an in vitro study of dissolution. *Urology* **2000,** *55* (1), 17-21.

29. Tiselius, H. G., New horizons in the management of patients with cystinuria. *Current Opinion in Urology* **2010,** *20* (2), 169-73.

30. Katz, A. K., Glusker, J. P., Beebe, S. A., & Bock, C. W., Calcium ion coordination: a comparison with that of beryllium, magnesium, and zinc. *Journal of the American Chemical Society* **1996,** *118* (24), 5752-5763.

31. Ernst, E., Chelation therapy for peripheral arterial occlusive disease: a systematic review. *Circulation* **1997,** *96* (3), 1031-1033.

32. Rathmann, K. L., & Golightly, L. K., Chelation therapy of atherosclerosis. *Drug Intelligence & Clinical Pharmacy* **1984,** *18* (12), 1000-1003.

33. Chutipongtanate, S., Chaiyarit, S., & Thongboonkerd, V., Citrate, not phosphate, can dissolve calcium oxalate monohydrate crystals and detach these crystals from renal tubular cells. *European Journal of Pharmacology* **2012,** *689* (1), 219-25.

34. Chung, J., Sosa, R., & Rimer, J. D., Elucidating the Effects of Polyprotic Acid Speciation in Calcium Oxalate Crystallization. *Crystal Growth & Design* **2017,** *17* (8), 4280-4288.

35. Scales, C. D., Smith, A. C., Hanley, J. M., & Saigal, C. S., Prevalence of kidney stones in the United States. *European Urology* **2012,** *62* (1), 160-165.

36. Burns, J. R., & Cargill, J. G., Kinetics of dissolution of calcium oxalate calculi with calcium-chelating irrigating solutions. *The Journal of Urology* **1987,** *137* (3), 530-3.

37. Ziolkowski, F., & Perrin, D. D., Dissolution of urinary stones by calcium-chelating agents: A study using a model system. *Investigative Urology* **1977,** *15* (3), 208-211.

38. Craddock, H. A., Caird, S., Wilkinson, H., & Guzzman, M., A new class of "green" corrosion inhibitors: Development and application. *SPE Projects, Facilities & Construction*, **2007,** *2* (04), 1-8.

39. Schweinsberg, M., Hater, W., & Verdes, J., New stable biodegradable scale inhibitor formulations for cooling water: development and field tests. *In 64th International Water Conference, Pittsburgh, PA* **2003,** *23*.

40. Cho, K. R., Salter, E. A., De Yoreo, J. J, Wierzbicki, A., Elhadj, S., Huang, Y., & Qiu, S. R., Growth inhibition of calcium oxalate monohydrate crystal by linear aspartic acid enantiomers investigated by in situ atomic force microscopy. *Crystal Engineering and Materials* **2013,** *15* (1), 54-64.

41. Kane, M. H., Rodman, J.S., Horten, B., Reckler, J., Marion, D., & Vaughan, E.D., Urothelial injury from ethylenediaminetetraacetic acid used as an irrigant in the urinary tract. *The Journal of Urology* **1989,** *142* (5), 1359-60.

42. Thuppil, V., & Tannir, S. , Treating lead toxicity: possibilities beyond synthetic chelation. *Journal of Krishna Institute of Medical Sciences University* **2013,** *2* (1), 4-31.

43. Weaver, M. L., Qiu, S. R., Hoyer, J. R., Casey, W. H., Nancollas, G. H., & De Yoreo, J. J., Improved model for inhibition of pathological mineralization based on citrate–calcium oxalate monohydrate interaction. *Journal of Chemical Physics and Physical Chemistry* **2006,** *7* (10), 2081-2084.

44. Hug, S., Grohe, B., Jalkanen, J., Chan, B., Galarreta, B., Vincent, K., Lagugné-Labarthet, F., Lajoie, G., Goldberg, H.A., Karttunen, M. & Hunter, G.K., Mechanism of inhibition of calcium oxalate crystal growth by an osteopontin phosphopeptide. *Soft Matter* **2012,** *8* (4), 1226-1233.

45. Sheng, X., Jung, T., Wesson, J. A., & Ward, M. D., Adhesion at calcium oxalate crystal surfaces and the effect of urinary constituents. *Proceedings of the National Academy of Sciences of the United States of America* **2005,** *102* (2), 267-272.

46. Shang, Y. F., Xu, M., Zhang, G.N., & Ouyang, J.M., Concave urinary crystallines: direct evidence of calcium oxalate crystals dissolution by citrate in vivo. *Bioinorganic Chemistry and Applications* **2013** ,*10* (1), 1155.

47. Farmanesh, S., Ramamoorthy, S., Chung, J., Asplin, J.R., Karande, P., & Rimer, J.D., Specificity of growth inhibitors and their cooperative effects in calcium oxalate monohydrate crystallization. *Journal of the American Chemical Society* **2013,** *136* (1), 367-76.

48. Chung, J., Granja, I., Taylor, M.G., Mpourmpakis, G., Asplin, J.R., & Rimer, J.D., Molecular modifiers reveal a mechanism of pathological crystal growth inhibition. *Nature* **2016,** *536* (7617), 446-50.

49. Escribano, J., Balaguer, A., Pagone, F., Feliu, A., & Roqué i Figuls, M. , Pharmacological interventions for preventing complications in idiopathic hypercalciuria. *The Cochrane Library* **2009,** *10* (1), 1002.

50. Tracy, C. R., & Pearle, M.S., Update on the medical management of stone disease. *Current Opinion in Urology* **2009,** *19* (2), 200-4.

51. Nancollas, G. H., & Gardner, G.L., Kinetics of crystal growth of calcium oxalate monohydrate. *Journal of Crystal Growth* **1974,** *21* (2), 267-76.

52. Echigo, T., Kimata, M., Kyono, A., & Shimizu, M., Re-investigation of the crystal structure of whewellite [Ca (C_2O_4)· H_2O] and the dehydration mechanism of caoxite [Ca (C_2O_4)· $3H_2O$]. *Mineralogical Magazine* **2005,** *69* (1), 77-78.

53. Tazzoli, V., & Domeneghetti, C., The crystal structures of whewellite and weddellite: re-examination and comparison. *American Mineralogist* **1980,** *65* (3-4), 327-34.

54. Deganello, S., Kampf, A.R., & Moore, P.B., The crystal structure of calcium oxalate trihydrate; $CaC_2O_4.3H_2O$. *American Mineralogist* **1981,** *66* (6-7), 859-65.

55. Hochrein, O., Thomas, A., & Kniep, R, Revealing the crystal structure of anhydrous calcium oxalate, $Ca[C_2O_4]$, by a combination of atomistic simulation and Rietveld

refinement. *Zeitschrift für anorganische und allgemeine Chemie* **2008,** *634* (11), 1826-1829.

56. Qiu, S. R., Wierzbicki, A., Orme, C.A., Cody, A.M., Hoyer, J.R., Nancollas, G.H., Zepeda, S., & De Yoreo, J.J., Molecular modulation of calcium oxalate crystallization by osteopontin and citrate. *Proceedings of the National Academy of Sciences* **2004,** *101* (7), 1811-5.

57. Chung, J., Granja I, Taylor MG, Mpourmpakis G, Asplin JR, & Rimer J. D., Inhibition of Calcium Oxalate Monohydrate Crystallization Using Organic Growth Modifiers *(Master dissertation, University of Houston)* **2013**.

58. Ouyang, J. M., & Deng, S. P., Controlled and uncontrolled crystallization of calcium oxalate monohydrate in the presence of citric acid. *Dalton Transactions* **2003,** *14* 2846-2851.

59. Kulaksizoglu, S., Sofikerim, M., & Cevik, C., Impact of various modifiers on calcium oxalate crystallization. *International Journal of Urology* **2007,** *14* (3), 214-218.

60. Adobes-Vidal, M., Shtukenberg, A. G., Ward, M. D., & Unwin, P. R., Multiscale Visualization and Quantitative Analysis of l-Cystine Crystal Dissolution. *Crystal Growth & Design* **2017,** *17* (4), 1766-1774.

61. Hillner, P. E., Manne, S., Gratz, A. J., & Hansma, P. K., AFM images of dissolution and growth on a calcite crystal. *Ultramicroscopy* **1992,** *42* 1387-1393.

62. Guo, S., Ward, M. D., & Wesson, J. A., Direct visualization of calcium oxalate monohydrate crystallization and dissolution with atomic force microscopy and the role of polymeric additives. *Langmuir* **2002,** *18* (11), 4284-4291.

63. Aljuhani, N. S., A calcium oxalate phase stability and dissolution study *(Masters dissertation, Rutgers University-Camden Graduate School)* **2017**.

64. Obaid, A., Non-droplet based microfluidic devices for calcium oxalate crystallization *(Masters dissertation, Rutgers University-Camden Graduate School)* **2016**.

65. Hames, A. D., Biochemistry labfax. *Academic Press* **2014,** *Chambers, J. A. A., & Rickwood, D.*, Colombus, OH 43212.

66. Perrin, D. D., Dissociation Constants of Organic Bases in Aqueous Solution *Butterworths London* **1972**, p.1965.

67. Serjeant, E. P., & Dempsey, B., Ionisation constants of organic acids in aqueous solution *Pergamon* **1979,** *23*.

68. Sillen, L. G., Martell, A. E., & Bjerrum, J., Stability constants of metal-ion complexes. *Chemical Society* **1964,** *541* (224).

69. White, D. J., Coyle-Rees, M., & Nancollas, G. H., Kinetic factors influencing the dissolution behavior of calcium oxalate renal stones: a constant composition study. *Calcified Tissue International* **1988,** *43* (5), 319-327.

70. Yang, Q., Dissolution mechanisms: theoretical and experimental investigations. *(Doctoral dissertation, University of Iowa)* **2015**.

71. Noyes, A. A., & Whitney, W. R., The rate of solution of solid substances in their own solutions. *Journal of the American Chemical Society* **1897,** *19* (12), 930-934.

72. Nernst, W., Theorie der Reaktionsgeschwindigkeit in heterogenen Systemen. *Zeitschrift für physikalische Chemie* **1904,** *47* (1), 52-55.

73. Brunner, E., Reaktionsgeschwindigkeit in heterogenen Systemen *Zeitschrift für physikalische Chemie* **1904,** *47* (1), 56-102.

74. Wurster, D. E., & Taylor, P. W., Dissolution rates. *Journal of Pharmaceutical Sciences* **1965,** *54* (2), 169-175.

75. Dokoumetzidis, A., Papadopoulou, V., Valsami, G., Macheras, P., Development of a reaction limited model of dissolution: Application to official dissolution tests experiments. *International Journal of Pharmaceutics* **2008,** *355*, 114-125.

76. Wang, J., Modeling and experimental evaluation of spherical particle dissolution *(Doctoral dissertation, University of Iowa)* **2002**.

77. Rickard, D., & Sjoeberg, E. L., Mixed kinetic control of calcite dissolution rates. *American Journal of Science* **1983,** *283* (8), 815-830.

78. White, D. J., & Nancollas, G. H., The kinetics of dissolution of calcium oxalate monohydrate; a constant composition study. *Journal of Crystal Growth* **1982,** *57* (2), 267-272.

79. McComas, W. H. J., & Rieman, W., The solubility of calcium oxalate monohydrate in pure water and various neutral salt solutions at 25ºC. *Journal of the American Chemical Society* **1942,** *64* (12), 2946-2947.

80. McComas, W. H. J., & Rieman, W., The Effect of pH on the Solubility of Calcium Oxalate. *Journal of the American Chemical Society* **1942,** *64* (12), 2948-2949.

81. Kallistratos, G., Litholytic agents: Preventive and curative drugs for nephrolithiasis. *In Drug Design* **1973,** *4*, 237-283.

82. Verplaetse, H., Verbeeck, R. M. H., Minnaert, H., & Oosterlinck, W., Solubility of inorganic kidney stone components in the presence of acid-base sensitive complexing agents. *European Urology* **1985,** *11*, 44-51.

83. Miller, G. H., Vermeulen, C. W., & Moore, J. D., Calcium oxalate solubility in urine: Experimental urolithiasis XIV. *The Journal of Urology* **1958,** *79* (3), 607-612.

84. Flora, S. J. S., Mittal, M., & Mehta, A., Heavy metal induced oxidative stress & its possible reversal by chelation therapy. *Indian Journal of Medical Research* **2008,** *128* (4), 501.

85. Lamas, G. A., Goertz, C., Boineau, R., Mark, D.B., Rozema, T., Nahin, R.L., Lindblad, L., Lewis, E.F., Drisko, J., Lee, K.L. & TACT Investigators., Effect of disodium EDTA chelation regimen on cardiovascular events in patients with previous myocardial infarction: the TACT randomized trial. *Jama* **2013,** *309* (12), 1241-1250.

86. Borden, T. A., & Lyon, E. S., The effects of magnesium and pH on experimental calcium oxalate stone disease. *Investigative Urology* **1969,** *6* (4), 412.

87. Desmars, J. F., & Tawashi, R., Dissolution and growth of calcium oxalate monohydrate I. Effect of magnesium and pH. *Biochimica et Biophysica Acta (BBA)-General Subjects* **1973,** *313* (2), 256-267.

88. Streit, J., Tran-Ho, L. C., & Königsberger, E., Solubility of the three calcium oxalate hydrates in sodium chloride solutions and urine-like liquors. *Monatshefte für Chemie/Chemical Monthly* **1998,** *129* (12), 1225-1236.

89. Ulmgren, P., & Radestrom, R., An equilibrium model of the solubility of calcium oxalate in sodium chloride medium. *Nordic Pulp & Paper Research Journal* **1999,** *14* (3), 214-220.

90. Dean, J. A., Lange's handbook of chemistry *Material and manufacturing process* **1990,** *5* (4), 8.82-8.102.

91. Windbergs, M., & Weitz, D. A., Drug Dissolution Chip (DDC): a microfluidic approach for drug release. *Small* **2011,** *7* (21), 3011-3015.

92. Ojovan, M. I., & Lee W.B., Connectivity and glass transition in disordered oxide systems. *Journal of Non-Crystalline Solids* **2010,** *356* (44), 2534-40.

93. Magnuson, M., Andersson, M., Lu, J., Hultman, L., & Jansson, U., Electronic structure and chemical bonding of amorphous chromium carbide thin films. *Journal of Physics: Condensed Matter.* **2012,** *24* (22), 225004.

94. Datta, S., & Grant, D. J., Crystal structures of drugs: advances in determination, prediction and engineering. *Nature Reviews Drug Discovery* **2004,** *3* (1), 42-57.

95. Healy, A. M., Worku, Z.A., Kumar, D., & Madi, A.M., Pharmaceutical Solvates, Hydrates and Amorphous Forms. *Advanced Drug Delivery Reviews* **2017,** *13092* (1), 22.

96. Grant, D. J., Theory and origin of polymorphism. *Drugs and the Pharmaceutical Sciences* **1999,** *95*, 1-33.

97. Yu, L., Amorphous pharmaceutical solids: preparation, characterization and stabilization. *Advanced Drug Delivery Reviews* **2001,** *48* (1), 27-42.

98. Vippagunta, S. R., Brittain, H. G., & Grant, D. J., Crystalline Solids. *Advanced Drug Delivery Reviews* **2001,** *48* (1), 3-26.

99. Grimm, U., Aperiodic crystals and beyond. Acta Crystallographica Section B: Structural Science. *Crystal Engineering and Materials* **2015,** *71* (3), 258-274.

100. Senechal, M., Structures beyond superspace. Acta Crystallographica Section B: Structural Science. *Crystal Engineering and Materials* **2015,** *71* (3), 250-1.

101. Brittain, H. G., & Grant, D. J., Effects of polymorphism and solid-state solvation on solubility and dissolution rate. *Polymorphism in Pharmaceutical Solids* **1999,** *95*, 279-330.

102. Johnson, D. A., Some Thermodynamic Aspects of Inorganic Chemistry. *Cambridge University Press* **1982,** *2nd ed.*

103. Smart, L. E., & Moore, E.A., Solid state chemistry: an introduction. *CRC Press Taylor and Francis Group, NW* **2012,** *3rd Ed*, 24.

104. Hiller, H., Crystallography and cohomology of groups. *The American Mathematical Monthly* **1986,** *93* (10), 765-779.

105. Fletcher, D. A., McMeeking, R.F., & Parkin, D., The United Kingdom Chemical DatabaseService. *Journal of Chemical Information and Computer Sciences* **1996,** *36*, 746–9.

106. Amjad, Z., & Demadis, K.D., Mineral Scales and Deposits: Scientific and Technological Approaches. *Elsevier, Amsterdam* **2015**, 239-319.